In silico screening of GMQ-like compounds reveals guanabenz and sephin1 as new allosteric modulators of acid-sensing ion channel 3

Gerard Callejo, Luke A. Pattison, Jack C. Greenhalgh, Sampurna Chakrabarti, Evangelia Andreopoulou, James R. F. Hockley, Ewan St. John Smith* and Taufiq Rahman*.

Department of Pharmacology, University of Cambridge, Tennis Court Road, Cambridge CB2 1PD, UK

**Corresponding authors: Ewan St. John Smith, es336@cam.ac.uk and Taufiq Rahman, mtur2@cam.ac.uk.*

Keywords: acid-sensing ion channel, GMQ, Sephin1, nociception

Abstract

Acid-sensing ion channels (ASICs) are voltage-independent cation channels that detect decreases in extracellular pH. Dysregulation of ASICs underpins a number of pathologies. Of particular interest is ASIC3, which is recognised as a key sensor of acid-induced pain and is instrumental in the establishment of pain arising from inflammatory conditions, such as rheumatoid arthritis. Thus, the identification of new ASIC3 modulators and the mechanistic understanding of how these compounds modulate ASIC3 could be important for the development of new strategies to counteract the detrimental effects of dysregulated ASIC3 activity in inflammation. Here, we report the identification of novel ASIC3 modulators based on the ASIC3 agonist, 2-guanidine-4-methylquinazoline (GMQ). Through a GMQ-guided *in silico* screening of Food and Drug administration (FDA)-approved drugs, 5 compounds were selected and tested for their modulation of rat ASIC3 (rASIC3) using whole-cell patch-clamp electrophysiology. Of the chosen drugs, guanabenz (GBZ), an α_2-adrenoceptor agonist, produced similar effects to GMQ on rASIC3, activating the channel at physiological pH (pH 7.4) and potentiating its response to mild acidic (pH 7) stimuli. Sephin1, a GBZ derivative that lacks α_2-adrenoceptor activity, has been proposed to act as a selective inhibitor of a regulatory subunit of the stress-induced protein phosphatase 1 (PPP1R15A) with promising therapeutic potential for the treatment of multiple sclerosis. However, we found that like GBZ, sephin1 activates rASIC3 at pH 7.4 and potentiates its response to acidic stimulation (pH 7), i.e. sephin1 is a novel modulator of rASIC3. Furthermore, docking experiments showed that, like GMQ, GBZ and sephin1 likely interact with the nonproton ligand sensor domain of rASIC3. Overall, these data demonstrate the utility of computational analysis for identifying novel ASIC3 modulators, which can be validated with electrophysiological analysis and may lead to the development of better compounds for targeting ASIC3 in the treatment of inflammatory conditions.

1. Introduction

Extracellular protons modulate the activity of a wide range of ion channels and receptors, which activate sensory neurons involved in nociception and the development of pain [1]. One key group of proton sensors is the acid-sensing ion channel (ASIC) family. These voltage-independent, ligand-gated cation channels are activated by extracellular protons [2–4] and belong to the amiloride-sensitive epithelial sodium channel/degenerin (ENaC/DEG) ion channel family [5,6]. In mammals, four genes (ASIC1-4 for human and asic1-4 for rodents) encode for at least 6 different ASIC subunits (ASIC1a, ASIC1b, ASIC2a, ASIC2b, ASIC3, ASIC4), which can assemble into homo- and heterotrimeric channels displaying different pH sensitivity, current kinetics and pharmacology [7–9]. ASICs are widely expressed in the central and peripheral nervous systems [2,10] and are implicated in a range of physiological and pathological processes including nociception, mechanosensation and learning/memory [11–21]. The involvement of ASICs in such a plethora of physiological and pathological roles makes them attractive pharmacological targets for drug development and a variety of agents have been identified that act as agonists/antagonists for these channels with differing levels of selectivity [22]. Of the ASIC subunits, there is good evidence that ASIC3 is a critical acid sensor involved in acid-induced pain. ASIC3 homomers are the most sensitive to decreases in extracellular pH [7], in response to which they produce a biphasic inward current composed of a large, rapidly desensitizing transient current, followed by a smaller, non-desensitizing sustained window current (resulting from an overlap between pH-dependent activation and inactivation curves) that lasts for the duration of the acidic stimulus [23,24]. Although protons appear to be the main endogenous activators of ASICs, other molecules that modulate ASIC function have been discovered. For instance, endogenous molecules such as arachidonic acid and anandamide [25], serotonin [26], dynorphins [27] and lactate [28] all enhance ASIC3 currents in response to acidic stimulation. In addition, 2-guanidine-4-methylquinazoline (GMQ) [29], agmatine [30] and lysophosphatidylcholine [31] can activate ASIC3 at physiological pH (pH 7.4) by increasing the sustained, window current. Moreover, a range of toxins isolated from animal venoms also modulate ASIC function [32]. Among them, APETx2, a toxin isolated from the sea anemone

Anthopleura elegantissima, inhibits the transient component of ASIC3 activation in response to an acidic stimulus (pH 4) without affecting its sustained component [33] and it has been used to establish the role of ASIC3 in a number of physiological and pathological processes, including inflammatory pain [12]. Nevertheless, the relationship between ASIC3, pain and inflammation is complex. Several histological studies, as well as those employing pharmacological ASIC3 modulation, have determined an involvement of ASIC3 in pain elicited in deep tissues such as joints, muscle and the viscera [34–40]. However, further studies using ASIC3-deficient mice have suggested a more limited role in pain [41], as well as a proposed dual role of ASIC3 in arthritis where lack of ASIC3 ameliorates pain, but increases inflammatory processes in the arthritic joint [42]. A possible explanation of these controversial results could be that inflammatory processes are sometimes [43], but not always [44], accompanied by acidosis. Nevertheless, the complex and controversial role of ASIC3 in some inflammatory processes requires the development of better pharmacological tools to dissect its precise function in such conditions. To this end, in the present study we hypothesised that we could employ GMQ as a query structure in a ligand-based *in silico* screening of FDA-approved drugs to identify novel ASIC3 modulators. From the results of the screening, we selected five different compounds with chemical and structural similarities to GMQ. From all drugs tested, (GBZ), an antihypertensive drug, caused an enhancement of acid-induced rASIC3 activation and, like GMQ, it also activated the channel at physiological pH. Given that GBZ is an agonist of α_2-adrenoceptors [45], and with the goal of identify a more selective ASIC3 modulator, we evaluated the effect of sephin1, a GBZ derivative that has no adrenoceptor activity and may be of use in protein misfolding diseases such as multiple sclerosis [46]. Similarly to GBZ and GMQ, sephin1 activated rASIC3 at pH 7.4 and potentiated its activation in response to a mild acidosis. In summary, we demonstrate that ligand-based *in silico* approaches can be useful to identify novel small molecule modulators of ASIC3. Indeed, we have identified, from a library of FDA-approved drugs that have been proven safe for their use in humans, novel ASIC3 modulators that enhance rASIC3 activity, proving that this approach can serve to identify potential new ASICs modulating drugs that could be useful in the treatment of inflammatory disorders.

111 # *2.* Materials and Methods

112 ## 2.1. Ligand-based screening

113 The 3D structure of GMQ was obtained from pubchem (pubchem CID: 345657)
114 and was subsequently energy-minimised using MMFF94 force field implemented
115 in OpenBabel version 2.4.0 [47]. Using the energy-minimised GMQ structure as
116 a 3D query, Rapid Overlay of Chemical Structures (ROCS) (version 3.2.2.2,
117 OpenEye Scientific Software, Santa Fe, NM) [48] was used to screen a conformer
118 library generated from eDrug3D database [49] that contains 1884 different
119 molecular structures including structures of enantiomers and of active
120 metabolites of FDA-approved drugs. The conformer library was generated using
121 Omega 3.0.1.2 (OpenEye Scientific Software) [50]. For each alignment, ROCS
122 compares 3D shape and chemical similarity and returns a Tanimoto Combo (TC)
123 score, ranging from 0 to 2, that includes a Shape Tanimoto (maximum 1) and
124 Colour Tanimoto (scaled colour score, maximum 1) [51]. Following manual
125 inspection of the top 150 hits ranked by the TC score, a subset of drugs was
126 selected for experimental testing. Molecular field-based alignment [52] of drug
127 structures with GMQ was performed using Forge (v 10.4.2; Cresset®, Litlington,
128 Cambridgeshire, UK).

129 ## 2.2. Chinese hamster ovary cell culture and transfection

130 Chinese hamster ovary (CHO) cells (Sigma, passage 6 to 20) were chosen for
131 this study due to the absence of endogenous ASIC-like currents [53] and were
132 grown using standard procedures in the following medium: Ham's F-12 Nutrient
133 Mixture (Life Technologies), 10 % fetal bovine serum (Sigma), 1 %
134 Penicillin/Streptomycin (100 U/ml, Life Technologies). 24-hours before
135 transfecting cells, 35 mm dishes (Fisher) were coated with 100 µg/ml poly-L-
136 lysine (Sigma) and cells from a 70-80% confluent flask were trypsinised,
137 resuspended in 5 ml CHO medium and a volume was taken to seed cells at a
138 1:10 dilution (2 ml/dish). For transfections, an EGFP expression vector was used
139 to enable identification of transfected cells and DNA was transfected at a ratio of
140 20:1 (rASIC3:GFP), using 1.5 µg rASIC3 DNA and 0.075 µg EGFP DNA; the

141 transfection reagent Lipofectamine LTX (Life Technologies) was used according
142 to the manufacturer's protocol.
143

144 2.3. Whole-cell electrophysiology

145 Whole-cell patch clamp recordings from CHO cells were performed at room
146 temperature 24-hours after transfection. For all the experiments, the intracellular
147 solution contained (in mM) 110 KCl, 10 NaCl, 1 $MgCl_2$, 1 EGTA, 10 HEPES, 2
148 Na_2ATP, 0.5 Na_2GTP in MilliQ water; pH was set to pH 7.3 by adding KOH and
149 the osmolality was adjusted to 310-315 mOsm with sucrose. The extracellular
150 solution contained (in mM) 140 NaCl, 4 KCl, 2 $CaCl_2$, 1 $MgCl_2$, 10 HEPES, 4
151 Glucose in MilliQ water; osmolality was adjusted to 300-310 mOsm with sucrose
152 and pH was adjusted to 7.4 with NaOH. Patch pipettes were pulled from glass
153 capillaries (Hilgenberg) using a Model P-97, Flaming/Brown puller (Sutter
154 Instruments) and had a resistance of 4-8 MΩ. Data were acquired using an
155 EPC10 amplifier (HEKA) and Patchmaster software (HEKA) after suitable
156 resistance compensation. To measure the effect of the different selected
157 compounds on rASIC3 current amplitude and inactivation time constant the
158 following protocol was used. After 5 s of pH 7.4 solution, pH 7 or pH 6 was applied
159 for 5 s to determine the baseline rASIC3 response. Then, in the first group of
160 experiments, after the initial pH 7 baseline rASIC3 response, compounds were
161 applied at pH 7 after 30 s of pH 7.4 to measure the effect of the selected
162 compounds on pH 7 rASIC3 activation. In the second group of experiments, a
163 second pH 6 application was performed after 10 s of pH 7.4 and 30 s of compound
164 application to determine the effect of these compounds on rASIC3 pH 6 response.
165 Finally, a third 5 s pH 6 or pH 7 application was performed after 30s of pH 7.4
166 solution to determine reversibility of any possible effect of the compounds on the
167 channel. For concentration-response recordings of GMQ, guanabenz and
168 sephin1 at pH 7.4 and pH 7 (sephin1), increasing concentrations of each drug (1
169 μM - 1 mM) were applied for 10 s with a 30 s wash period with extracellular pH
170 7.4 solution between each application. For pH-response recordings, extracellular
171 solutions with a pH ranging from 7.4 to 5 with/without sephin1 were applied for
172 10 s with a 30 s wash period between applications. All compounds/acidic

173 solutions were applied to cells through a gravity-driven 12-barrel perfusion
174 system [54]. In all the experiments the holding potential was set at -60mV.
175

176 2.4. Molecular modelling and docking

177 We used three homology models of rASIC3 (Uniprot accession: O35240) based
178 on published structures of chicken ASIC1 as the templates, solved in its closed
179 (PDB id: 6AVE; [55]), open (PDB id: 4NTW; [56]) and desensitized state (PDB
180 id: 2QTS; [8]) and we designated the rASIC3 models as 'rASIC3-closed', 'rASIC3-
181 open' and 'rASIC3-desensitized', respectively. Detail of the model building was
182 previously reported [57]. Selected drugs were docked to the rASIC3 models using
183 the Lamarckian genetic algorithm (LGA) implemented in AutoDock 4.2.6 [58]. For
184 all docking, an unbiased ("blind") docking approach [59] was used where the
185 entire trimers of rASIC3 models were used for generating the grid map in
186 AutoGrid, without assuming a priori any putative binding site(s) for the ligands.
187 The docking protocol was semi-flexible i.e. only the ligand structures were
188 allowed to be fully flexible whilst the protein structures were held rigid. Prior to
189 docking, structures of all drugs (obtained from PubChem) and the rASIC3 trimer
190 were prepared using the AutoDock Tools. Five independent docking runs were
191 performed for each drug and the pose associated with the highest reproducibility
192 and lowest predicted free energy of interaction (ΔG, kcal/mol) was considered as
193 the final pose for each drug. From those final docked poses of the drugs, the
194 corresponding 2D ligand interaction diagrams were generated using PoseView™
195 implemented in the ProteinsPlus webserver (https://proteins.plus/). Although only
196 the top-ranked pose for each molecule was considered for analysing the residue
197 contacts through Poseview, representative top 1-5 poses for each drug has been
198 shown in Fig. 7. UCSF Chimera version 1.14 (http://www.rbvi.ucsf.edu/chimera/)
199 was used for all molecular representations.
200

201 2.5. Drugs

202 All the small molecules used in this study were purchased from Sigma
203 (Gilliangham, UK) except for tizanidine (Tocris, Bristol, UK) and APETx2
204 (Smartox, Saint egrève, France). Stock solutions were made at 100 mM for
205 tizanidine (in H_2O), guanabenz (EtOH), cycloguanil (DMSO) and sephin1

206 (DMSO), 50 mM for GMQ (DMSO) and brimonidine (H_2O), and 40 mM for
207 guanfacine (H_2O). For most experiments, compounds were diluted in pH 7.4 or
208 pH 7 extracellular solution at 500 μM, however, GMQ, guanabenz and sephin1
209 were also diluted in extracellular pH 7.4 (or pH 7 for sephin1) solution at different
210 concentrations. An APETx2 stock solution was made at 100 μM and diluted at 1
211 μM in pH 7.4 extracellular solution.
212

213 ## 2.6. Data analysis

214 Absolute peak amplitudes were measured by subtracting the peak amplitude
215 response from the 5-second mean baseline prior to stimulation. Peak amplitude
216 was then normalised by dividing the absolute peak amplitude by the capacitance
217 of the cell to obtain peak current density (pA/pF). The inactivation time constant
218 was measured with a single exponential equation using a built-in function of
219 Fitmaster. The sustained current to transient current ratio was calculated by
220 measuring the size of the sustained current (peak sustained response at the end
221 of the stimulus minus the 5- or 10-second mean baseline current; expressed as
222 I_{5s} or I_{10s}) and dividing this value by the peak amplitude current (I_{5s}/I_{peak} x 100).
223 The analysis of rASIC3 current amplitudes and kinetics was performed as
224 previously reported [9]. Statistical analysis was performed in GraphPad Prism
225 using a paired t-test comparing the baseline pH response (pA/pF) against the pH
226 response after compound application for each cell. Data were plotted as a
227 percentage of the initial pH response for each cell. In order to compare the
228 difference between the rASIC3 activation of GMQ, GBZ and sephin1 at pH 7.4,
229 results were expressed as a percentage of the initial pH 6 baseline ASIC3
230 response and unpaired t-test or one-way ANOVA with Holm-Sidak's multiple
231 comparison test was used. For concentration-response curves, all
232 measurements were expressed as a percentage of the pH baseline peak current
233 value (pH 6 or pH 7). For pH-response curves, all measurements were
234 transformed to percent of the maximum peak current (I/Imax x 100). The EC_{50} for
235 both concentration- and pH-response (pH_{50}) experiments were determined using
236 a standard Hill equation using GraphPad Prism. For the pH-response curve in the
237 presence of sephin1 a biphasic equation was used in GraphPad Prism. For the
238 analysis of pH-dependent effect of sephin1 on the rASIC3 sustained current a

239 Gaussian distribution equation was used in GraphPad Prism. All results are
240 expressed as mean ± standard error of the mean (SEM). All figures were made
241 using GraphPad Prism and Adobe Illustrator CS6.

3. Results

3.1. Ligand-based *in silico* screening of novel ASIC3 modulators

Using the energy-minimised 3D structure of GMQ as a query, we used ROCS to screen a conformer library of FDA-approved drugs (eDrug3D) [49]. ROCS aligns each conformer from the target chemical library against the query or bait structure and quantifies the overall similarity between the aligned ligands as the Tanimoto Combo (TC) score. The latter is the sum of the Shape Tanimoto and the Color Tanimoto (scaled colour score), which represent the measure of similarity in 3D shape and chemical properties between the aligned moieties, respectively [51]. Of the top 150 hits ranked by the TC score, we manually inspected each individual hit for the degrees of 3D shape overlap and chemical similarity with GMQ, paying particular attention to the presence of a guanidine (or similar) moiety. This finally led us to shortlist 5 drugs, namely tizanidine (TIZ), cycloguanil (CG), brimonidine (BRI), guanfacine (GF) and GBZ (Fig. 1A). Of these hits, GBZ and GF contain an explicit (i.e. free) guanidine group (shown in red in Fig.1B), whereas CG, BRI and TIZ have an 'implicit' (i.e. within a ring) guanidine moiety.

To assess how these drugs compare to GMQ in terms of overall surface electrostatics, they were aligned to the energy-minimised GMQ structure using the software Forge™ (Cresset, UK), which uses a proprietary molecular mechanics-based ('XED') forcefield to generate and compare molecular 'field points' between aligned molecules (Fig. 1B). These field points represent positions of maximum interaction of a molecule with its electrostatic, steric and hydrophobic surroundings and thus effectively provides a 'protein-centric' view of a ligand. Upon alignment, Forge produces a field similarity score that takes both volume and molecular field points into account and a field score >0.7 is often regarded as indicator of reasonably good electrostatic similarities between the query and the bait molecule [52]. GBZ both qualitatively and quantitatively has the highest field point similarity with GMQ; in decreasing order of similarity of molecular fields, compound similarity with GMQ was computed as: GBZ > BRI > TIZ > GF > CG (Fig. 1B).

275 ## 3.2. Effect of selected drugs on acid-induced rASIC3 activation.

276 The following set of experiments were conducted to determine if the selected
277 drugs modulate rASIC3 function. We performed whole-cell patch clamp
278 recordings in CHO cells co-transfected with rASIC3 and EGFP and evaluated the
279 effect of each one of the drugs selected on the response of rASIC3 to pH 7 and
280 pH 6. Millimolar concentrations of GMQ are required to activate rASIC3 channels
281 at pH 7.4, but at micromolar concentrations, GMQ sensitises pH 7-induced
282 rASIC3 channel activation [29]. First, we evaluated the effect of each drug (500
283 μM) on rASIC3 when applied at pH 7. The prototypic ASIC3 agonist GMQ induced
284 an increase in the transient (I_{Peak}, Fig. 2A-B and table 1, n = 9, paired t-test, p =
285 0.001) sustained current (I_{5s}, Fig. 2A and table 1, n = 9, paired t-test, p = 0.0012),
286 and the ratio I_{5s}/I_{Peak} (Fig 2C and Table 1, n = 9, paired t-test, p < 0.0001),
287 suggesting a stronger effect in the sustained component of rASIC3 pH 7
288 activation. Among the drugs selected (summarised in Table 1 and Fig. 2A-C), TIZ
289 and GBZ produced a similar effect, inducing and increase in all three parameters
290 (Fig. 2A-C; TIZ: I_{Peak}, n = 9, paired t-test, p = 0.0006; I_{5s}, n = 9, paired t-test, p =
291 0.0022; I_{5s}/I_{Peak} n = 9, paired t-test, p = 0.01: GBZ: I_{Peak}, n = 9, paired t-test, p =
292 0.038; I_{5s}, n = 9, paired t-test, p = 0.012; I_{5s}/I_{Peak} n = 9, paired t-test, p = 0.0012).
293 On the contrary, CG induced a slight but still significant inhibition of the transient
294 rASIC3 current activation without affecting the sustained component or the ratio
295 I_{5s}/I_{Peak} (CG: I_{Peak}, n = 8, paired t-test, p = 0.0061; I_{5s}, n = 8, paired t-test, p = 0.2;
296 I_{5s}/I_{Peak} n = 8, paired t-test, p = 0.15). GF and BRI induced contrary effects on the
297 I_{5s}/I_{Peak} ratio, whilst GF produce an enhancement of this parameter, suggesting a
298 stronger enhancement of the sustained component, BRI induced an inhibition
299 (GF: I_{5s}/I_{Peak} n = 9, paired t-test, p = 0.03; BRI: I_{5s}/I_{Peak} n = 6, paired t-test, p =
300 0.007).
301
302 We next tested the effect of the pre-application (30 s) of each drug (500 μM) on
303 the rASIC3 response to pH 6. In this series of experiments, we also evaluated
304 the effect of GMQ and APETx2, which were used as positive controls. As
305 expected, in rASIC3-expressing CHO cells, APETx2 (1 μM) application did not
306 activate the channel at physiological pH (pH 7.4), but produced a significant
307 inhibition of transient (I_{Peak}, Fig. 2D-E, n = 10, paired t-test, p = 0.0013) and

308 sustained (I_{5s} in Fig. 2A, n = 10, paired t-test, p = 0.029) current evoked by pH
309 6 (Table 2). However, the ratio I_{5s}/I_{Peak} was significantly increased (Fig 2F and
310 Table 2, n = 10, paired t-test, p = 0.036), indicating that the predominant APETx2
311 inhibitory effect is exerted on the transient phase as previously described [33]. In
312 addition, APETx2 significantly accelerated the inactivation time constant (Tau) of
313 rASIC3 (Fig. 2G and Table 2, n = 10, paired t-test, p = 0.0005). By contrast, GMQ
314 generated a sustained inward current at pH 7.4 as reported previously [29], but
315 did not significantly modulate channel current amplitude or inactivation kinetics
316 (Table 2).
317
318 Among the 5 drugs tested in these series of experiments (summarised in Table
319 2), with the exception of GBZ, none of them produced a significant change on
320 rASIC3 current amplitude or inactivation kinetics (Fig. 2E-G). Unlike all other
321 compounds tested, and in a similar fashion to GMQ, we observed that GBZ, a
322 drug currently used to treat hypertension, activated rASIC3 at physiological pH
323 (Fig. 2D). However, unlike GMQ, pre-application of GBZ elicited a significant
324 increase in the transient and sustained components of the pH 6-induced rASIC3
325 current (Fig. 2E, I_{Peak}, n = 11, paired t-test, p = 0.0173; I_{5s}, n = 11, paired t-test, p
326 = 0.015). The stronger potentiating effect upon the sustained current (303%)
327 compared with the effect on the transient current (13%) produced a significant
328 increase in the I_{5s}/I_{Peak} ratio (Fig. 2F, n = 11, paired t-test, p = 0.016) and the
329 inactivation time constant of the pH 6-induced rASIC3 response was significantly
330 increased by GBZ (Fig. 2G, n = 11, paired t-test, p = 0.014).
331

332 3.3. GBZ activates rASIC3 at physiological pH and likely binds 333 to the nonproton ligand sensor domain.

334 Given that GBZ was the only selected drug able to activate rASIC3 at pH 7.4 and
335 potentiate its response to pH 7 and pH 6, we decided to investigate further the
336 mechanism action of GBZ on rASIC3. In order to quantify the rASIC3 activation
337 at physiological pH observed by GBZ, we performed electrophysiological
338 recordings and compared the results to the effects observed with GMQ. At pH
339 7.4 , even though both GMQ and GBZ (1 mM), are capable of activating rASIC3,
340 the activation of rASIC3 by GBZ is of significantly of smaller magnitude compared

341 to GMQ-induced rASIC3 activation (10.8 ± 1.76 % for GMQ vs 5.06 ± 1.04 for
342 GBZ, Fig.3A and 3B, unpaired t-test, n = 12-13, p = 0.0061).
343
344 Given the structural and chemical similarities between GMQ and GBZ (Fig. 1),
345 we next performed docking experiments to elucidate the binding mechanism of
346 GBZ to rASIC3. The carboxyl-carboxylate interaction pair formed by the residues
347 E79 and E423 in the palm domain of rASIC3 has been implicated in GMQ binding
348 and the cavity where these two amino acids are localised has been named the
349 'nonproton ligand sensor domain' because several 'nonproton' ASIC3 ligands
350 such as GMQ, agmatine and serotonin all bind this domain [26,29,30]. Although
351 GBZ shares certain structural and chemical properties with GMQ, including a
352 guanidine moiety (Fig. 1B), these molecules may or may not share the same
353 binding site or manifest similar binding mode to the same site on ASIC3. Besides,
354 the precise binding mode of any 'nonproton' ASIC3 ligand including GMQ to the
355 nonproton ligand sensor domain is likely to be influenced by the state of ASIC3,
356 since some local structural changes, though subtle, can be observed in the lower
357 palm region of overlaid chicken ASIC1 structures solved in closed, open and
358 desensitized states (Fig. 3C) and this has been highlighted in a recent review
359 [60].
360
361 To address all these aspects, we performed *in silico* blind docking experiments
362 with GMQ and GBZ against our three rASIC3 homology models (designated as
363 rASIC3-closed, rASIC3-open and rASIC3-desensitized) that were made using
364 template chicken ASIC1 structures solved at closed [55], open [56] and
365 desensitized states [8], respectively. In our unbiased docking approach, GMQ
366 preferentially docked to a pocket located in the palm domain of all three rASIC3
367 models (Fig.3D, 3F and 3H) which has been computationally and experimentally
368 established in previous studies as the likely binding site for GMQ and designated
369 as the nonproton ligand sensor domain [29,61]. However, subtle differences in its
370 proposed binding mode were noticed in rASIC3-closed (Fig. 3D), rASIC3-open
371 (Fig. 3F) and rASIC3-desensitized (Fig.3H) models. The 2D ligand interaction
372 diagrams for GMQ docked to those rASIC3 models show 4-methylquinazoline
373 moiety makes a hydrophobic interaction with L77 and V425 in all 3 rASIC3
374 models but for rASIC3-closed model (Fig 3E), two additional residues namely

375 E79 and L273 seem also to participate. Interestingly, the guanidinium moiety of
376 GMQ seems to form two salt bridges with two E423 residues present in the same
377 or in different monomeric subunits in case with rASIC3-closed (Fig. 3E) and
378 rASIC3-desensitized (Fig. 3I) structures, respectively whilst for the rASIC3-open
379 model, E423 of one subunit is replaced by E79 in making such salt bridge (Fig.
380 3G). GBZ also docked to the same location and it broadly retains similar
381 interactions (Fig. 3E, 3G and 3I). Like GMQ, its mode of interaction also seems
382 to vary depending on the rASIC3 model. For example, its guanidinium moiety
383 makes two salt bridges with E423 of a single monomer (for rASIC3-closed, Fig.
384 3E), E423 and Q271 of different monomers (for rASIC3-open, Fig. 3G) and E423
385 from two different monomers (for rASIC3-desensitized, Fig. 3I). Also, no or fewer
386 hydrophobic contacts were noticeable for GBZ in all rASIC3 models (L77 in
387 rASIC3-closed model and Q269 in rASIC3-desensitized model), presumably due
388 to lack of an additional aromatic ring when compared to GMQ structure (Fig. 3E,
389 3G and 3I).
390
391 Taken together, these results indicate that GBZ modulates rASIC3 in the mild
392 acidic range and that its binding site likely overlaps with that of GMQ, the so called
393 nonproton ligand sensor domain. However, their precise modes of binding may
394 be different and can be subjected to further variations depending on the state of
395 the channel, which may underlie the different potency and efficacy observed on
396 rASIC3 current activation.
397

398 ## 3.4. The GBZ derivative, sephin1, positively modulates rASIC3

399 Recently, it has been demonstrated that a GBZ derivative without α_2-
400 adrenoceptor activity, sephin1 (also known as IFB-088; Fig.4A) acts as an
401 inhibitor of a regulatory subunit of the stress-induced protein phosphatase 1
402 (PPP1R15A) [62]. Sephin1 is effectively the mono-chlorinated version of GBZ
403 and is currently under investigation in clinical trials and hence was not included
404 in the eDrug3D database that we initially screened with ROCS using GMQ as
405 bait. ROCS-based alignment of sephin1 with GMQ revealed by far the highest
406 similarity among the 5 initially selected FDA-approved compounds in terms of
407 both 3D shape (>90%) and chemical features (>50%) with an overall TC score of

408 1.481 (Fig. 4A). In agreement with this, sephin1 appeared to be the most similar
409 to GMQ among all FDA-approved selected drugs in terms of the molecular field
410 points with the highest overall field score (Field Score = 0.847, Fig. 4B).
411
412 Given the high molecular similarity observed *in silico* for sephin1 and GMQ/GBZ,
413 we evaluated the effect of sephin1 on the acid-induced rASIC3 response. Firstly,
414 we observed that sephin1 (500 μM) did not affect the transient component of pH
415 6-induced rASIC3 activation, similar to the effect observed for GMQ but unlike
416 GBZ (Fig. 2E and table 2), however it did induce an increase in the amplitude of
417 the sustained component (I_{peak}, Fig. 4C-D and table 2, n = 10, paired t-test, p =
418 0.82; I_{5s}, Fig. 4C-D and table 2, n = 10, paired t-test, p = 0.03) without significantly
419 affecting the I_{5s}/I_{peak} ratio (I_{5s}/I_{peak}, Fig. 4C-D and table 2, n = 10, paired t-test, p
420 = 0.13) or the inactivation time constant (Tau, Fig. 4C-D and table 2, n = 10,
421 paired t-test, n = 10, p = 0.09, Fig. 4C). When comparing the effect of sephin1,
422 GBZ and GMQ on the pH 6 ASIC3 response, we did not observe significant
423 differences in the transient phase of ASIC3 activation, however, we did observe
424 a significantly bigger increase in the sustained component after GBZ in
425 comparison to GMQ (GMQ, 11.4 ± 7.96 % vs GBZ, 303.07 ± 107.1 %, F(2,26) =
426 3.420, t(26) = 2.567, ANOVA, Holm-Sidak's multiple comparison test, p =
427 0.0483). Similarly to GMQ and GBZ, 500 μM and 1 mM sephin1 also activated
428 rASIC3 at pH 7.4 (Fig. 4C and 4E insets), however, sephin1's activation, as with
429 that observed for GBZ, was significantly smaller than GMQ ASIC3 activation at
430 pH 7.4 (GMQ, 10.8 ± 1.76 % vs GBZ, 5.06 ± 1.04 %, F(2,34) = 5.673, t(34) =
431 3.423, ANOVA, Holm-Sidak's multiple comparison test, p = 0.0033; GMQ, 10.8 ±
432 1.76 % vs sephin1, 3.32 ± 0.8 %, F(2,34) = 5.673, t(34) = 4.42, ANOVA, Holm-
433 Sidak's multiple comparison test, p = 0.0003). In order to compare the efficacy
434 and potency of all three molecules on their action on rASIC3 at pH 7.4, we
435 performed a concentration-response (CR) analysis. Due to a limitation in the
436 solubility of the drugs in their solvent, we could not perform a full CR experiment,
437 but nevertheless, we could compare the effect of all three molecules estimating
438 the lowest EC_{50} value. GMQ appears to be the most efficacious of all three
439 molecules, showing an activation of 10.8 ± 1.76 % at 1 mM (% of pH 6 initial
440 response) (Fig. 4F), whereas at the same concentration of GBZ and sephin1
441 elicited an activation of 5.06 ± 1.04 % and 3.32 ± 0.8 %, respectively (Fig. 4F

442 inset). On the other hand, GBZ appears to be the most potent of all three
443 molecules with an estimated EC_{50} of 67.5 μM, compared to 0.68 mM and 1.22
444 mM for GMQ and sephin1, respectively (Fig. 4F inset). Even though sephin1
445 appears to be the least potent and efficacious of all three molecules, like GMQ
446 and GBZ, sephin1 induced a strong sensitisation, in a concentration-dependent
447 fashion, of the transient and sustained (I_{10s} in Fig.5D and 5H) components of the
448 pH 7-induced rASIC3 activation (Fig. 5A-D), revealing an EC_{50} of 28.93 μM for
449 the rASIC3 transient current at pH 7 (Fig. 5B). At 500 μM, like GMQ and GBZ,
450 sephin1 also enhanced the transient and sustained currents of rASIC3 (I_{peak} 87.58
451 ± 37.33 pA/pF vs $I_{peak\ sephin1}$ 230.84 ± 80.42 pA/pF n = 9, paired t-test, p = 0.016;
452 I_{5s} 27.13 ± 18.65 pA/pF vs $I_{5s\ sephin1}$ 148.37 ± 64.98 pA/pF, n = 9, paired t-test, p
453 = 0.03; I_{5s}/I_{peak} 30.24 ± 6.8 % vs $I_{5s\ sephin1}$ 65.19 ± 6.54 % n = 9, paired t-test, p <
454 0.0001), however, we found no significant differences in the sensitisation of
455 ASIC3 pH 7 response between all three molecules. Given the high similarities in
456 the action of sephin1 and GMQ, we hypothesized that sephin1 also binds to the
457 nonproton ligand sensor domain of rASIC3. We next tested the pH dependency
458 of rASIC3 modulation by sephin1. The application of different pH solutions
459 ranging from pH 7.4 to 5 (Fig. 5G and 5H) on rASIC3 induced currents of
460 increasing magnitude to produce a sigmoidal curve that could be fitted to reveal
461 a pH_{50} value of 6.36 (Fig. 5G inset), in accordance with previous reports [7,9].
462 However, in the presence of sephin1 (500 μM), rASIC3 transient activation
463 followed a pH-dependent, biphasic curve (Fig. 5H inset), suggesting an interplay
464 between the action of sephin1 on rASIC3 and its proton activation. As showed
465 previously by Yu et al. using GMQ [29], sephin1 activated rASIC3 at pH 7.4, but
466 also potentiated its sustained current at all pH solutions tested, showing a
467 Gaussian distribution with a peak at pH 6.56 (r^2 = 0.43, Fig. 5I). Similarly to GBZ,
468 *in silico* blind docking experiments against all rASIC3 models suggest that the
469 E423 but not the E79 of the nonproton ligand sensor domain engages in salt
470 bridge interaction with the guanidinium moiety of sephin1. The aromatic ring of
471 sephin1 can have possible hydrophobic interactions with residue A378, L77,
472 E423 and E269 (Fig. 6B, 6D and 6F), depending on the nature of the rASIC3
473 model. Altogether, these results show that sephin1 modulates rASIC3 activation
474 possibly through interacting with the nonproton ligand sensor domain of the
475 channel.

4. Discussion

The ASIC family of ion channels have been implicated in many physiological and pathological processes including nociception [14,19,63], where they have been established as attractive pharmacological targets for treating pain. ASIC3 is of particular interest given its high expression in primary sensory neurones [10] and its involvement in inflammatory pain originating from different tissues including muscle, joints and skin [12,34,35,64–66]. Therefore, the exploration of novel ASIC3 modulators could increase our knowledge of ion channel function and also be pivotal for the development of new strategies to counteract the detrimental effects of dysregulated ASIC3 activity in pathophysiological states. Many molecules that modulate ASIC3 function have been discovered, ranging from non-selective ASIC3 blockers such as amiloride that acts as a pore blocker and paradoxically stimulates ASIC3 at pH 7.4 [3], to more specific molecules, such as the inhibitory toxin APETx2, which inhibits the acid-induced transient ASIC3 current [33] but also inhibits $Na_V1.8$ channels [67], and the agonist GMQ, which activates ASIC3 at pH 7.4 and potentiates its activation in response to an acidic stimulus through the nonproton ligand sensor domain of ASIC3 [29,61]. However, GMQ is not a specific agonist of ASIC3 as several studies have demonstrated that GMQ also modulates other ASIC subunits [68,69] as well as $GABA_A$ receptors [70]. In the present study, we used a ligand-based *in silico* screening of FDA-approved drugs to identify novel rASIC3 modulators. Of the top 150 hits ranked by TC score, we selected 5 different drugs with the highest structural and chemical resemblance to GMQ (Fig. 1A), including the presence of a guanidine group. Using an independent algorithm implemented in Cresset's Forge™, we then aligned these 5 drugs with GMQ and compared their surface electrostatic properties represented by the molecular field points. Of the selected drugs, GBZ showed a striking resemblance to GMQ with regard to surface electrostatics and this was reflected in the highest observed value for the field score (0.80). However, the surface electrostatic analysis of sephin1 resulted in an even higher resemblance to GMQ with a field score of 0.847. Of the remaining 4 drugs, only BRI, which had the 2nd best field score, showed some degree of electrostatic similarity with GMQ (Fig.1B).

509 We next sought to experimentally evaluate the effects of these drugs on acid-
510 induced rASIC3 activation. Several drugs showed a modulation of the rASIC3 pH
511 7 response (Fig. 2A-C), however, among them only one showed a modulatory
512 effect on rASIC3 acid response to pH 6, namely GBZ, an α_2-adrenoceptor
513 agonist. When compared to GMQ, GBZ exhibited a high TC score (1.086) (Fig.
514 1B) and the highest molecular field score (0.8) among the FDA-approved drugs
515 selected (Fig. 1), together with the presence of an explicit guanidine group.
516 Interestingly, TIZ that showed a higher TC score (Fig. 1A; 1.047) and a lower field
517 score (Fig. 1B) in terms of surface electrostatics than GBZ did enhance only the
518 pH 7 but not the pH 6 rASIC3 response. The precise reason for such behaviour
519 of TIZ remains to be properly investigated but it indicates that a free guanidinium
520 moiety is perhaps important to influence the pH 6 ASIC3 response which TIZ
521 clearly lacks, unlike GBZ and GMQ. Indeed, a pseudo or implicit form of the
522 guanidinium moiety contained in the 4,5-dihydro-1*H*-imidazol-2-amine ring of TIZ
523 appears to be significantly less electropositive than the free guanidinium moiety
524 present in GMQ and GBZ (Fig. 1B) and it is therefore likely to be less able to
525 serve as a H-bond donor during its recognition at the ASIC3, which could underlie
526 its differential response.
527
528 Given the overall 3D and electrostatic similarity of GBZ with GMQ (Fig.1), it was
529 perhaps unsurprising to observe that GBZ followed a similar mode of action to
530 GMQ, being capable of activating rASIC3 at pH 7.4 (Fig. 2A and 3A) and inducing
531 a non-desensitising inward current but showing a higher potency but less efficacy
532 than GMQ (Fig. 4F). Based on our findings from the blind docking experiments
533 against the rASIC3-closed homology model (Fig. 3D and 3E), this difference
534 could be explained by the lack of interaction with the core residue E79 and the
535 adjacent residues V425 and L273. Such interactions are observed for GMQ in
536 our docking experiment (Fig. 3E) and have been previously shown to be
537 important in the hydrophobic interaction of the 4-methylquinazoline moiety of
538 GMQ [61]. This is plausible because, unlike GMQ, GBZ lacks a second aromatic
539 moiety in an appropriate position to allow such hydrophobic contacts to be
540 established. Moreover, the sensitisation of the pH 6-induced rASIC3 activation
541 observed by GBZ (Fig. 2D-G), but not by GMQ, could result from different residue
542 interactions (Q271 and G269) of both molecules with rASIC3.

543

544 GBZ is an orally active α_2-adrenoceptor agonist that has been used for many
545 years as an antihypertensive drug [71]. However, GBZ also binds to the
546 regulatory subunit of protein phosphatase 1, PPP1R15A, disrupting the stress-
547 induced dephosphorylation of the α subunit of the translation initiation factor 2
548 (eIF2α), which protects against the detrimental accumulation of misfolded
549 proteins in the endoplasmic reticulum (ER) [72] and has been proven effective in
550 animal models that mimic misfolding protein diseases such as multiple sclerosis
551 [73]. A recent study has identified a mono-chlorinated version of GBZ, sephin1,
552 which retains the GBZ PPP1R15A inhibition activity, but without adrenoceptor
553 activity [62] and it has also been shown to be effective in animal models of
554 amyotrophic lateral sclerosis [62], Charcot-Marie-Tooth 1B (CMT1B) neuropathy
555 [62] and multiple sclerosis [46]. Given the efficacy of sephin1 to ameliorate the
556 pathogenesis of misfolding protein diseases, InFlectis Bioscience has begun the
557 Phase I clinical trials to evaluate the safety of sephin1 (IFB-088) with the aim of
558 evaluating its effect on the treatment of Charcot-Marie-Tooth 1B (CMT1B)
559 disorder.

560

561 As a result of the similar pharmacological profile of GBZ to GMQ and with the
562 intention of identifying a more selective rASIC3 modulator without adrenoceptor
563 activity, we tested the effect of sephin1 on acid-induced rASIC3 activation. We
564 observed that sephin1 shared a similar pharmacological profile with GBZ and
565 GMQ, sensitising the response (sustained component) of rASIC3 to low pH (pH
566 6) (Fig. 4C and 4D) and mild acidosis (pH 7) (Fig. 5A-D), and activating rASIC3
567 at pH 7.4 (Fig.4E). These results were consistent with our expectations given that
568 sephin1 appeared to be most similar to GMQ in terms of structural and chemical
569 properties, exhibiting the highest TC score (Fig. 4A), and the highest molecular
570 field points score (Fig. 4B). Moreover, increasing concentrations of sephin1
571 induced increasing potentiation of the transient and sustained phases of the pH
572 7-induced rASIC3 activation (Fig. 5A). In our blind docking experiments, carried
573 out multiple times against three different ASIC3 models in open, closed and
574 desensitized states, sephin1 poses tend to reproducibly cluster to the same site
575 i.e. the nonproton ligand sensor domain where the GMQ and GBZ poses also
576 cluster (Fig.7). Close inspection of the corresponding ligand interaction diagrams

577 of sephin1 poses indicate that similar to GMQ and GBZ, the negatively charged
578 residue E423 is likely to interact with the explicit guanidinium group of sephin1 in
579 all three ASIC3 functional states (Fig. 6B, 6D and 6F). However, compared to
580 GBZ, sephin1's lack of a chloride atom in the aromatic ring seems to allow it to
581 make hydrophobic interactions with surrounding residues like A378 (ASIC3-
582 desensitised model, Fig. 6F), Q269 (ASIC3-open model, Fig. 6D) and L77
583 (rASIC3-closed model, Fig. 6B) from the adjacent subunit, but not with V425 as
584 observed for GMQ (Fig.3E, 3G and 3I). Overall, these interactions likely underlie
585 differential recognition of sephin1 at the nonproton ligand sensor domain of
586 ASIC3, compared to that of GMQ and GBZ. GMQ is able to activate human
587 ASIC3 (hASIC3) at neutral pH [74]. Given the structural and chemical similarities
588 between GMQ, GBZ and sephin1, the close similarity between the nonproton
589 ligand sensor domain in rASIC3 and hASIC3 (core residues E79 and E423, and
590 adjacent residues, L77, Q269, L273, A378 and V425 are identical in both
591 sequences [61]) and the predicted similar binding modes of all three molecules,
592 it is likely that GBZ and sephin1 will also be able to modulate human ASIC3.
593
594 Sephin1 is able to selectively disrupt the PPP1R15A-PP1c complex at 50 μM in
595 cells *in vitro*, and after oral administration (1 or 10mg/kg) sephin1 accumulates in
596 the nervous system reaching concentrations of up to 1 μM in the brain and sciatic
597 nerve [62]. Moreover, a continuous 2-week treatment with sephin1 at 100 nM
598 (once every 2 days) has shown efficacy in rescuing myelination of the dorsal root
599 ganglia in a mouse model that mimics Charcot-Marie-Tooth 1B (CMT1B) in
600 humans. Given the high functional expression of rASIC3 in DRG neurones and
601 its involvement in pain derived from inflammatory diseases, together with the
602 action of sephin1 observed on the channel, it is possible that sephin1 treatment
603 could induce and/or exacerbate pain due to the activation of ASIC3 in DRG
604 neurones, however our results show that both activation of rASIC3 at
605 physiological pH (pH 7.4) and potentiation of the response to mild acidosis (pH
606 7) require higher concentrations of sephin1 (Fig. 4F and 5A) than those observed
607 to be beneficial in treating misfolding protein diseases in mice. However, the
608 possible additive effects of ASIC3 activated by sephin1 and other endogenous
609 molecules found in the inflammatory soup such as arachidonic acid, which also
610 potentiates the acid-induced response of ASIC3 [25] cannot be excluded.

611 Moreover, ASICs function as trimers, displaying different pharmacological
612 profiles depending upon subunit composition. In the present study, we have not
613 evaluated the effect of sephin1 on heteromeric ASIC3-containing channels or
614 other homomeric ASIC channels, and therefore, we cannot fully hypothesise what
615 the potential effects of sephin1 *in vivo* might be. For instance, GMQ modulates
616 ASIC1a and ASIC1b by shifting their pH dependence of activation to more acidic
617 values [75], precisely the opposite effect seen for ASIC3, an effect attributed to
618 structural differences in the extracellular domain of ASIC1a/b and ASIC3 [69].
619 Given the pharmacological and structural resemblance of sephin1 to GMQ, it is
620 possible that sephin1 induces similar modulatory effects on other ASIC subunits.
621 Nevertheless, we believe that the evaluation of pain thresholds in mice and
622 humans used to study the effect of sephin1 in misfolding protein disease should
623 be considered in future studies.
624
625 In summary, we have identified new rASIC3 modulators using a ligand-based *in*
626 *silico* approach, namely GBZ and sephin1, and evaluated their effect on rASIC3
627 function using electrophysiology. Here we provide proof of principle, using a size-
628 restricted chemical library (i.e. FDA-approved drug library), but believe this
629 approach can be exploited in the future to screen much larger chemical space,
630 enabling the identification of novel chemical scaffolds that act as ASIC
631 modulators.

Acknowledgements

The authors declare no competing financial interests. This work was supported by Versus Arthritis Research Grants (RG20930 and RG21973; GC and EStJS), BBSRC grant (BB/R006210/1; JRFH and EStJS), BBSRC-funded studentships (LAP and JCG, BB/M011194/1) and Gates Cambridge Trust (SC). TR gratefully acknowledges OpenEye Scientific Software and Cresset for granting academic licenses for some software used in the present study.

Author Contributions

GC designed the research, conducted the experiments, acquired and analysed the data and wrote the manuscript. LAP, JCG, SC, EA and JRFH acquired and analysed the data. TR and EStJS designed the research and wrote the manuscript. All authors approved the final version of the manuscript.

Declaration of Conflicting Interests

The authors have no conflicting interests to declare.

648 # References

649

650 [1] L.A. Pattison, G. Callejo, E. St John Smith, Evolution of acid nociception:
651 ion channels and receptors for detecting acid, Philos. Trans. R. Soc. B. 374
652 (2019). doi:10.1098/rstb.2019.0291.
653 [2] S. Kellenberger, L. Schild, International Union of Basic and Clinical
654 Pharmacology. XCI. Structure, Function, and Pharmacology of Acid-
655 Sensing Ion Channels and the Epithelial Na+ Channel., Pharmacol. Rev.
656 67 (2015) 1–35. doi:10.1124/pr.114.009225.
657 [3] R. Waldmann, G. Champigny, F. Bassilana, C. Heurteaux, M. Lazdunski,
658 A proton-gated cation channel involved in acid-sensing, Nature. 386 (1997)
659 173–177.
660 [4] S. Gründer, M. Pusch, Biophysical properties of acid-sensing ion channels
661 (ASICs), Neuropharmacology. 94 (2015) 9–18.
662 doi:10.1016/j.neuropharm.2014.12.016.
663 [5] E. Deval, E. Lingueglia, Acid-Sensing Ion Channels and nociception in the
664 peripheral and central nervous systems, Neuropharmacology. 94 (2015)
665 49–57. doi:10.1016/j.neuropharm.2015.02.009.
666 [6] S. Gründer, M. Pusch, Neuropharmacology Biophysical properties of acid-
667 sensing ion channels (ASICs), Neuropharmacology. (2015) 1–10.
668 doi:10.1016/j.neuropharm.2014.12.016.
669 [7] M. Hesselager, pH Dependency and Desensitization Kinetics of
670 Heterologously Expressed Combinations of Acid-sensing Ion Channel
671 Subunits, J. Biol. Chem. 279 (2004) 11006–11015.
672 [8] J. Jasti, H. Furukawa, E.B. Gonzales, E. Gouaux, Structure of acid-sensing
673 ion channel 1 at 1.9 A resolution and low pH., Nature. 449 (2007) 316–23.
674 doi:10.1038/nature06163.
675 [9] L.-N. Schuhmacher, G. Callejo, S. Srivats, E.S.J. Smith, Naked mole-rat
676 acid-sensing ion channel 3 forms nonfunctional homomers, but functional
677 heteromers, J. Biol. Chem. 293 (2018) 1756–1766.
678 doi:10.1074/jbc.M117.807859.
679 [10] L.-N. Schuhmacher, E.S.J. Smith, Expression of acid-sensing ion channels
680 and selection of reference genes in mouse and naked mole rat, Mol. Brain.

681 9 (2016) 97. doi:10.1186/s13041-016-0279-2.
682 [11] G. Callejo, A. Castellanos, M. Castany, A. Gual, C. Luna, M.C. Acosta, J.
683 Gallar, J.P. Giblin, X. Gasull, Acid-sensing ion channels detect moderate
684 acidifications to induce ocular pain, Pain. 156 (2015) 483–495.
685 doi:10.1097/01.j.pain.0000460335.49525.17.
686 [12] E. Deval, J. Noël, N. Lay, A. Alloui, S. Diochot, V. Friend, M. Jodar, M.
687 Lazdunski, E. Lingueglia, ASIC3, a sensor of acidic and primary
688 inflammatory pain, EMBO J. 27 (2008) 3047–3055.
689 [13] S. Diochot, A. Baron, M. Salinas, D. Douguet, S. Scarzello, A.-S. Dabert-
690 Gay, D. Debayle, V. Friend, A. Alloui, M. Lazdunski, E. Lingueglia, Black
691 mamba venom peptides target acid-sensing ion channels to abolish pain,
692 Nature. (2012) 1–24.
693 [14] E. Deval, J. Noël, X. Gasull, A. Delaunay, A. Alloui, V. Friend, A. Eschalier,
694 M. Lazdunski, E. Lingueglia, Acid-sensing ion channels in postoperative
695 pain, J. Neurosci. 31 (2011) 6059–6066.
696 [15] S. Kang, J.H. Jang, M.P. Price, M. Gautam, C.J. Benson, H. Gong, M.J.
697 Welsh, T.J. Brennan, Simultaneous Disruption of Mouse ASIC1a, ASIC2
698 and ASIC3 Genes Enhances Cutaneous Mechanosensitivity, PLoS One. 7
699 (2012) e35225.
700 [16] A.J. Page, S.M. Brierley, C.M. Martin, C. Martinez-Salgado, J. a. Wemmie,
701 T.J. Brennan, E. Symonds, T. Omari, G.R. Lewin, M.J. Welsh, L.A.
702 Blackshaw, The ion channel ASIC1 contributes to visceral but not
703 cutaneous mechanoreceptor function, Gastroenterology. 127 (2004) 1739–
704 1747. doi:10.1053/j.gastro.2004.08.061.
705 [17] M.P. Price, G.R. Lewin, S.L. McIlwrath, C. Cheng, J. Xie, P. a Heppenstall,
706 C.L. Stucky, a G. Mannsfeldt, T.J. Brennan, H. a Drummond, J. Qiao, C.J.
707 Benson, D.E. Tarr, R.F. Hrstka, B. Yang, R. a Williamson, M.J. Welsh, The
708 mammalian sodium channel BNC1 is required for normal touch sensation.,
709 Nature. 407 (2000) 1007–11. doi:10.1038/35039512.
710 [18] M.P. Price, S.L. McIlwrath, J. Xie, C. Cheng, J. Qiao, D.E. Tarr, K. a Sluka,
711 T.J. Brennan, G.R. Lewin, M.J. Welsh, The DRASIC cation channel
712 contributes to the detection of cutaneous touch and acid stimuli in mice.,
713 Neuron. 32 (2001) 1071–83.
714 [19] M. Mazzuca, C. Heurteaux, A. Alloui, S. Diochot, A. Baron, N. Voilley, N.

715 Blondeau, P. Escoubas, A. Gélot, A. Cupo, A. Zimmer, A.M. Zimmer, A.
716 Eschalier, M. Lazdunski, A tarantula peptide against pain via ASIC1a
717 channels and opioid mechanisms, Nat. Neurosci. 10 (2007) 943–945.
718 [20] P. Zhang, Single Channel Properties of Rat Acid-sensitive Ion Channel-
719 1alpha, -2a, and -3 Expressed in Xenopus Oocytes, J. Gen. Physiol. 120
720 (2002) 553–566. doi:10.1085/jgp.20028574.
721 [21] L.-N. Schuhmacher, S. Srivats, E.S.J. Smith, Structural Domains
722 Underlying the Activation of Acid-Sensing Ion Channel 2a, Mol. Pharmacol.
723 87 (2015) 561–571. doi:10.1124/mol.114.096909.
724 [22] A. Baron, E. Lingueglia, Pharmacology of acid-sensing ion channels -
725 Physiological and therapeutical perspectives., Neuropharmacology. (2015)
726 1–17. doi:10.1016/j.neuropharm.2015.01.005.
727 [23] R. Waldmann, F. Bassilana, J. de Weille, G. Champigny, C. Heurteaux, M.
728 Lazdunski, Molecular Cloning of a Non-inactivating Proton-gated Na+
729 Channel Specific for Sensory Neurons, J. Biol. Chem. 272 (1997) 20975–
730 20978. doi:10.1074/jbc.272.34.20975.
731 [24] J. Yagi, H.N. Wenk, L. a Naves, E.W. McCleskey, Sustained currents
732 through ASIC3 ion channels at the modest pH changes that occur during
733 myocardial ischemia., Circ. Res. 99 (2006) 501–9.
734 doi:10.1161/01.RES.0000238388.79295.4c.
735 [25] E.S. Smith, H. Cadiou, P. a. McNaughton, Arachidonic acid potentiates
736 acid-sensing ion channels in rat sensory neurons by a direct action,
737 Neuroscience. 145 (2007) 686–698.
738 doi:10.1016/j.neuroscience.2006.12.024.
739 [26] X. Wang, W.-G. Li, Y. Yu, X. Xiao, J. Cheng, W.-Z. Zeng, Z. Peng, M. Xi
740 Zhu, T.-L. Xu, Serotonin facilitates peripheral pain sensitivity in a manner
741 that depends on the nonproton ligand sensing domain of ASIC3 channel.,
742 J. Neurosci. 33 (2013) 4265–79. doi:10.1523/JNEUROSCI.3376-12.2013.
743 [27] T.W. Sherwood, C.C. Askwith, Dynorphin opioid peptides enhance acid-
744 sensing ion channel 1a activity and acidosis-induced neuronal death., J.
745 Neurosci. 29 (2009) 14371–80. doi:10.1523/JNEUROSCI.2186-09.2009.
746 [28] D.C. Immke, E.W. McCleskey, Lactate enhances the acid-sensing Na+
747 channel on ischemia-sensing neurons., Nat. Neurosci. 4 (2001) 869–70.
748 doi:10.1038/nn0901-869.

749 [29] Y. Yu, Z. Chen, W.-G. Li, H. Cao, E.-G. Feng, F. Yu, H. Liu, H. Jiang, T.-L.
750 Xu, A nonproton ligand sensor in the acid-sensing ion channel., Neuron. 68
751 (2010) 61–72. doi:10.1016/j.neuron.2010.09.001.
752 [30] W.-G. Li, Y. Yu, Z.-D. Zhang, H. Cao, T.-L. Xu, ASIC3 channels integrate
753 agmatine and multiple inflammatory signals through the nonproton ligand
754 sensing domain., Mol. Pain. 6 (2010) 88. doi:10.1186/1744-8069-6-88.
755 [31] S. Marra, R. Ferru-clément, V. Breuil, A. Delaunay, M. Christin, V. Friend,
756 S. Sebille, C. Cognard, T. Ferreira, C. Roux, L. Euller-ziegler, J. Noel, E.
757 Lingueglia, E. Deval, Non-acidic activation of pain-related Acid-Sensing Ion
758 Channel 3 by lipids, EMBO J. 35 (2016) 1–15.
759 doi:10.15252/embj.201592335.
760 [32] B. Cristofori-Armstrong, L.D. Rash, Acid-sensing ion channel (ASIC)
761 structure and function: Insights from spider, snake and sea anemone
762 venoms, Neuropharmacology. 127 (2017) 173–184.
763 doi:10.1016/j.neuropharm.2017.04.042.
764 [33] S. Diochot, A. Baron, L.D. Rash, E. Deval, P. Escoubas, S. Scarzello, M.
765 Salinas, M. Lazdunski, A new sea anemone peptide, APETx2, inhibits
766 ASIC3, a major acid-sensitive channel in sensory neurons., EMBO J. 23
767 (2004) 1516–25. doi:10.1038/sj.emboj.7600177.
768 [34] W.S. Hsieh, C.C. Kung, S.L. Huang, S.C. Lin, W.H. Sun, TDAG8, TRPV1,
769 and ASIC3 involved in establishing hyperalgesic priming in experimental
770 rheumatoid arthritis, Sci. Rep. 7 (2017) 1–14. doi:10.1038/s41598-017-
771 09200-6.
772 [35] M. Ikeuchi, S.J. Kolker, L.A. Burnes, R.Y. Walder, K.A. Sluka, Role of
773 ASIC3 in the primary and secondary hyperalgesia produced by joint
774 inflammation in mice., Pain. 137 (2008) 662–9.
775 doi:10.1016/j.pain.2008.01.020.
776 [36] M. Ikeuchi, S.J. Kolker, K.A. Sluka, Acid-sensing ion channel 3 expression
777 in mouse knee joint afferents and effects of carrageenan-induced arthritis.,
778 J. Pain. 10 (2009) 336–42. doi:10.1016/j.jpain.2008.10.010.
779 [37] M. Izumi, M. Ikeuchi, Q. Ji, T. Tani, Local ASIC3 modulates pain and
780 disease progression in a rat model of osteoarthritis., J. Biomed. Sci. 19
781 (2012) 77. doi:10.1186/1423-0127-19-77.
782 [38] R.C.W. Jones, E. Otsuka, E. Wagstrom, C.S. Jensen, M.P. Price, G.F.

783 Gebhart, Short-term sensitization of colon mechanoreceptors is associated
784 with long-term hypersensitivity to colon distention in the mouse.,
785 Gastroenterology. 133 (2007) 184–94. doi:10.1053/j.gastro.2007.04.042.
786 [39] C. Reimers, C.-H. Lee, H. Kalbacher, Y. Tian, C.-H. Hung, A. Schmidt, L.
787 Prokop, S. Kauferstein, D. Mebs, C.-C. Chen, S. Grunder, Identification of
788 a cono-{RFamide} from the venom of {Conus} textile that targets {ASIC}3
789 and enhances muscle pain., Proc. Natl. Acad. Sci. U. S. A. 114 (2017)
790 E3507--E3515. doi:10.1073/pnas.1616232114.
791 [40] K.A. Sluka, R. Radhakrishnan, C.J. Benson, J.O. Eshcol, M.P. Price, K.
792 Babinski, K.M. Audette, D.C. Yeomans, S.P. Wilson, ASIC3 in muscle
793 mediates mechanical, but not heat, hyperalgesia associated with muscle
794 inflammation, Pain. 129 (2007) 102–112.
795 [41] A.A. Staniland, S.B. McMahon, Mice lacking acid-sensing ion channels
796 (ASIC) 1 or 2, but not ASIC3, show increased pain behaviour in the formalin
797 test., Eur. J. Pain. 13 (2009) 554–63. doi:10.1016/j.ejpain.2008.07.001.
798 [42] K. a Sluka, L. a Rasmussen, M.M. Edgar, J.M. O'Donnell, R.Y. Walder, S.J.
799 Kolker, D.L. Boyle, G.S. Firestein, Acid-sensing ion channel 3 deficiency
800 increases inflammation but decreases pain behavior in murine arthritis.,
801 Arthritis Rheum. 65 (2013) 1194–202. doi:10.1002/art.37862.
802 [43] D.J. Scholz, M.A. Janich, U. Kollisch, R.F. Schulte, J.H. Ardenkjaer-Larsen,
803 A. Frank, A. Haase, M. Schwaiger, M.I. Menzel, Quantified pH imaging with
804 hyperpolarized (13) C-bicarbonate., Magn. Reson. Med. 73 (2015) 2274–
805 2282. doi:10.1002/mrm.25357.
806 [44] A.J. Wright, Z.M.A. Husson, D.-E. Hu, G. Callejo, K.M. Brindle, E.S.J.
807 Smith, Increased hyperpolarized [1-(13) C] lactate production in a model of
808 joint inflammation is not accompanied by tissue acidosis as assessed using
809 hyperpolarized (13) C-labelled bicarbonate., NMR Biomed. 31 (2018)
810 e3892. doi:10.1002/nbm.3892.
811 [45] F.S.J. Tennant, R.A. Rawson, Guanabenz acetate: a new, long-acting
812 alpha-two adrenergic agonist for opioid withdrawal., NIDA Res. Monogr. 49
813 (1984) 338–343.
814 [46] Y. Chen, J.R. Podojil, R.B. Kunjamma, J. Jones, M. Weiner, W. Lin, S.D.
815 Miller, B. Popko, Sephin1, which prolongs the integrated stress response,
816 is a promising therapeutic for multiple sclerosis., Brain. 142 (2019) 344–

817 361. doi:10.1093/brain/awy322.
818 [47] N.M. O'Boyle, M. Banck, C.A. James, C. Morley, T. Vandermeersch, G.R.
819 Hutchison, Open Babel: An open chemical toolbox., J. Cheminform. 3
820 (2011) 33. doi:10.1186/1758-2946-3-33.
821 [48] P.C.D. Hawkins, A.G. Skillman, A. Nicholls, Comparison of shape-
822 matching and docking as virtual screening tools., J. Med. Chem. 50 (2007)
823 74–82. doi:10.1021/jm0603365.
824 [49] E. Pihan, L. Colliandre, J.-F. Guichou, D. Douguet, e-Drug3D: 3D structure
825 collections dedicated to drug repurposing and fragment-based drug
826 design., Bioinformatics. 28 (2012) 1540–1541.
827 doi:10.1093/bioinformatics/bts186.
828 [50] P.C.D. Hawkins, A.G. Skillman, G.L. Warren, B.A. Ellingson, M.T. Stahl,
829 Conformer generation with OMEGA: algorithm and validation using high
830 quality structures from the Protein Databank and Cambridge Structural
831 Database., J. Chem. Inf. Model. 50 (2010) 572–584.
832 doi:10.1021/ci100031x.
833 [51] E. Naylor, A. Arredouani, S.R. Vasudevan, A.M. Lewis, R. Parkesh, A.
834 Mizote, D. Rosen, J.M. Thomas, M. Izumi, A. Ganesan, A. Galione, G.C.
835 Churchill, Identification of a chemical probe for NAADP by virtual
836 screening., Nat. Chem. Biol. 5 (2009) 220–226. doi:10.1038/nchembio.150.
837 [52] T. Cheeseright, M. Mackey, S. Rose, A. Vinter, Molecular field extrema as
838 descriptors of biological activity: definition and validation, J. Chem. Inf.
839 Model. 46 (2006) 665–676. doi:10.1021/ci050357s.
840 [53] E.S.J. Smith, X. Zhang, H. Cadiou, P.A. McNaughton, Proton binding sites
841 involved in the activation of acid-sensing ion channel ASIC2a, Neurosci.
842 Lett. 426 (2007) 12–17.
843 [54] I. Dittert, J. Benedikt, L. Vyklický, K. Zimmermann, P.W. Reeh, V. Vlachová,
844 Improved superfusion technique for rapid cooling or heating of cultured
845 cells under patch-clamp conditions, J. Neurosci. Methods. 151 (2006) 178–
846 185. doi:10.1016/j.jneumeth.2005.07.005.
847 [55] N. Yoder, C. Yoshioka, E. Gouaux, Gating mechanisms of acid-sensing ion
848 channels., Nature. 555 (2018) 397–401. doi:10.1038/nature25782.
849 [56] I. Baconguis, C.J. Bohlen, A. Goehring, D. Julius, E. Gouaux, X-ray
850 structure of acid-sensing ion channel 1-snake toxin complex reveals open

851 state of a Na(+)-selective channel., Cell. 156 (2014) 717–29.
852 doi:10.1016/j.cell.2014.01.011.
853 [57] T. Rahman, E.S.J. Smith, In silico assessment of interaction of sea
854 anemone toxin APETx2 and acid sensing ion channel 3., Biochem.
855 Biophys. Res. Commun. 450 (2014) 384–9.
856 doi:10.1016/j.bbrc.2014.05.130.
857 [58] G.M. Morris, R. Huey, W. Lindstrom, M.F. Sanner, R.K. Belew, D.S.
858 Goodsell, A.J. Olson, AutoDock4 and AutoDockTools4: Automated docking
859 with selective receptor flexibility., J. Comput. Chem. 30 (2009) 2785–2791.
860 doi:10.1002/jcc.21256.
861 [59] B. Iorga, D. Herlem, E. Barre, C. Guillou, Acetylcholine nicotinic receptors:
862 finding the putative binding site of allosteric modulators using the “blind
863 docking” approach., J. Mol. Model. 12 (2006) 366–372.
864 doi:10.1007/s00894-005-0057-z.
865 [60] S. Vullo, S. Kellenberger, A molecular view of the function and
866 pharmacology of acid-sensing ion channels., Pharmacol. Res. (2019)
867 104166. doi:10.1016/j.phrs.2019.02.005.
868 [61] Y. Yu, W.-G.G. Li, Z. Chen, H. Cao, H. Yang, H. Jiang, T.-L. Le Xu, Atomic
869 level characterization of the nonproton ligand-sensing domain of ASIC3
870 channels, J. Biol. Chem. 286 (2011) 24996–25006.
871 doi:10.1074/jbc.M111.239558.
872 [62] I. Das, A. Krzyzosiak, K. Schneider, L. Wrabetz, M. D’Antonio, N. Barry, A.
873 Sigurdardottir, A. Bertolotti, Preventing proteostasis diseases by selective
874 inhibition of a phosphatase regulatory subunit, Science (80-.). 348 (2015)
875 239–242. doi:10.1126/science.aaa4484.
876 [63] J.-H. Lin, C.-H. Hung, D.-S. Han, S.-T. Chen, C.-H. Lee, W.-Z. Sun, C.-C.
877 Chen, Sensing acidosis: nociception or sngception?, J. Biomed. Sci. 25
878 (2018) 85. doi:10.1186/s12929-018-0486-5.
879 [64] C.-C. Chen, A. Zimmer, W.-H. Sun, J. Hall, M.J. Brownstein, A. Zimmer, A
880 role for ASIC3 in the modulation of high-intensity pain stimuli., Proc. Natl.
881 Acad. Sci. U. S. A. 99 (2002) 8992–7. doi:10.1073/pnas.122245999.
882 [65] W.-N. Chen, C.-C. Chen, Acid mediates a prolonged antinociception via
883 substance P signaling in acid-induced chronic widespread pain., Mol. Pain.
884 10 (2014) 30. doi:10.1186/1744-8069-10-30.

885 [66] J. Karczewski, R.H. Spencer, V.M. Garsky, A. Liang, M.D. Leitl, M.J. Cato,
886 S.P. Cook, S. Kane, M.O. Urban, Reversal of acid-induced and
887 inflammatory pain by the selective ASIC3 inhibitor, APETx2., Br. J.
888 Pharmacol. 161 (2010) 950–60. doi:10.1111/j.1476-5381.2010.00918.x.
889 [67] M.G. Blanchard, L.D. Rash, S. Kellenberger, Inhibition of voltage-gated
890 Na(+) currents in sensory neurones by the sea anemone toxin APETx2.,
891 Br. J. Pharmacol. 165 (2012) 2167–77. doi:10.1111/j.1476-
892 5381.2011.01674.x.
893 [68] O. Alijevic, H. Hammoud, A. Vaithia, V. Trendafilov, M. Bollenbach, M.
894 Schmitt, F. Bihel, S. Kellenberger, Heteroarylguanidines as Allosteric
895 Modulators of ASIC1a and ASIC3 Channels, ACS Chem. Neurosci. 9
896 (2018) 1357–1365. doi:10.1021/acschemneuro.7b00529.
897 [69] T. Besson, E. Lingueglia, M. Salinas, Pharmacological modulation of Acid-
898 Sensing Ion Channels 1a and 3 by amiloride and 2-guanidine-4-
899 methylquinazoline (GMQ), Neuropharmacology. 125 (2017) 429–440.
900 doi:10.1016/j.neuropharm.2017.08.004.
901 [70] X. Xiao, M.X. Zhu, T. Le Xu, 2-Guanidine-4-methylquinazoline acts as a
902 novel competitive antagonist of A type γ-aminobutyric acid receptors,
903 Neuropharmacology. 75 (2013) 126–137.
904 doi:10.1016/j.neuropharm.2013.07.018.
905 [71] B. Holmes, R.N. Brogden, R.C. Heel, T.M. Speight, G.S. Avery,
906 Guanabenz. {A} review of its pharmacodynamic properties and therapeutic
907 efficacy in hypertension., Drugs. 26 (1983) 212–229.
908 [72] P. Tsaytler, H.P. Harding, D. Ron, A. Bertolotti, Selective inhibition of a
909 regulatory subunit of protein phosphatase 1 restores proteostasis, Science.
910 332 (2011) 91–94. doi:10.1126/science.1201396.
911 [73] S.W. Way, J.R. Podojil, B.L. Clayton, A. Zaremba, T.L. Collins, R.B.
912 Kunjamma, A.P. Robinson, P. Brugarolas, R.H. Miller, S.D. Miller, B.
913 Popko, Pharmaceutical integrated stress response enhancement protects
914 oligodendrocytes and provides a potential multiple sclerosis therapeutic.,
915 Nat. Commun. 6 (2015) 6532. doi:10.1038/ncomms7532.
916 [74] D. Barth, M. Fronius, Shear force modulates the activity of acid-sensing ion
917 channels at low pH or in the presence of non-proton ligands., Sci. Rep. 9
918 (2019) 6781. doi:10.1038/s41598-019-43097-7.

919 [75] O. Alijevic, S. Kellenberger, Subtype-specific modulation of acid-sensing
920 ion channel (ASIC) function by 2-guanidine-4-methylquinazoline., J. Biol.
921 Chem. 287 (2012) 36059–70. doi:10.1074/jbc.M112.360487.
922

923 # 5. Figures/Table Legends

924 **Figure 1. Selected FDA-approved drugs after ligand-based in silico**
925 **screening using GMQ as query molecule.** (A) Representations of the selected
926 drugs showing similarity in 3D shape and chemical features with GMQ**.** Drugs
927 were chosen from ligand-based in silico screening using ROCS (OpenEye
928 Scientific Software) that ranked them on the basis of Tanimoto Combo Score.
929 The latter is a sum of Shape Tanimoto and Colour Tanimoto score indicating
930 similarity in 3D shape (maximum value = 1) and chemical features (maximum
931 value = 1). The volume of the query molecule (GMQ) is shown as a dotted area
932 and the chemical similarity aspects are shown in different colours. The figure was
933 generated by ROCS Report (OpenEye). (B) 2D chemical structure of GMQ and
934 selected FDA-approved drugs (Guanidine or similar moiety is shown in red) and
935 alignment of these drugs with GMQ based on molecular electrostatic field
936 potentials. Forge^{TM} (v 10.4.2; Cresset) was used to align the drug structures with
937 the energy-minimised structure of GMQ. In all cases, the negative, positive and
938 hydrophobic field points are coloured blue, red and gold, respectively (van der
939 Waals isosurfaces are not shown). The sphere size corresponds to possible
940 interaction strength with the cognate probe used for field point calculation. The
941 individual molecular field similarity scores to GMQ (maximum value = 1) are given
942 below right in each panel.
943

944 **Figure 2. Effect of the selected drugs rASIC3 response to pH 6**. (A) Example
945 traces of the effect for the 5 different selected drugs (500 μM) on pH 7-induced
946 rASIC3 activation together with example trace showing the effect of the prototypic
947 rASIC3 modulator GMQ (500 μM). In all cases drugs were applied at pH 7. (B-C)
948 Bar plots showing the effect of the selected drugs and GMQ on transient (peak)
949 (B) and the sustained current (expressed as the ratio I_{5s}/I_{peak}) (C). (D) Example
950 traces of the effect for the 5 different selected drugs (500 μM) on pH 6-induced
951 rASIC3 activation together with example traces showing the effect of known
952 rASIC3 modulators, APETx2 (1 μM) and GMQ (500 μM). In all cases drugs were
953 applied for 30 s prior to pH 6-induced rASIC3 activation. (B-D) Bar plots showing
954 the effect of the selected drugs, APETx2 and GMQ on transient (peak) (B) and

955 sustained current (C), and inactivation time constant (D) of rASIC3 activation. All
956 values were normalised to baseline pH 7 or pH 6 rASIC3 activation and
957 expressed as means ± SEM (n = 6-11, paired t-test, *p <0.05 and ***p ≤ 0.005 vs
958 baseline pH 7 or pH 6 activation).
959
960 **Figure 3. Effect of GBZ on rASIC3 response at physiological pH and**
961 **proposed binding site and binding mode of GBZ on rASIC3 closed, open**
962 **and desensitized models.**(A) Example traces of rASIC3 activation at
963 physiological pH (pH 7.4) elicited by GMQ (1 mM) and GBZ (1 mM). Inset showing
964 magnification of GBZ activation. (B) Bar plot showing the quantification of GMQ-
965 and GBZ-induced rASIC3 activation at pH 7.4 normalised against ASIC3 pH 6
966 response (n = 12-13, unpaired t-test, **p ≤ 0.01). (C) The structures of chicken
967 ASIC1a representing the closed (PDB id: 6AVE, coloured in pale blue), open
968 (PDB id: 4NTX, coloured in salmon) and desensitized (PDB id: 4NYK, coloured
969 in grey) are shown in cartoon representations and were overlaid using UCSF
970 Chimera 1.14. Various regions are indicated in canonical terms. (D, F and H)
971 Representative top-ranked poses of GMQ (red) and GBZ (green) obtained
972 through AutoDock 4.2.6-based blind docking against rASIC3-closed, rASIC3-
973 open and rASIC3-desensitized models, respectively, are shown. For clarity, only
974 two subunits of the channel are shown in cartoon representations (subunit A in
975 golden colour and subunit C in pale blue colour). A close-up view of the site and
976 the docked poses for each model is shown to the left. (E, G and I) PoseView™
977 derived ligand interaction diagrams for the docked poses of GMQ and GBZ are
978 shown. A and C indicate the two subunits of rASIC3.
979
980 **Figure 4. Effect of sephin1 on rASIC3 activation.** (A-B) Representation of
981 sephin1 showing similarity in 3D shape and chemical features with GMQ (A) and
982 molecular field electrostatics (B) as described in Fig.1 for selected drugs. (C)
983 Example trace of effect of sephin1 (500 μM) on pH6-induced rASIC3 activation.
984 (C inset) Magnification of rASIC3 activation induced by sephin1 at pH 7.4. (C) Bar
985 plot quantifying sephin1 effect on the transient and sustained normalised current
986 and inactivation time constant of the pH 6-induced rASIC3 activation expressed
987 as a percentage of the pH 6 baseline activation (n = 10, paired t-test; *p <0.05 vs
988 baseline pH 6 activation). (E) Example trace showing rASIC3 activation by

989 sephin1 at pH 7.4. (E inset) Magnification of the current elicited by sephin1 (n =
990 12). (F) Concentration-response effect of increasing concentrations of GMQ,
991 GBZ and sephin1 (1 μM–1 mM) applied at pH 7.4 on rASIC3. Absolute values
992 were normalised using the capacitance of each cell (pA/pF) and expressed as a
993 percentage of the pH 6-induced rASIC3 activation. A non-linear regression using
994 a sigmoidal function was used to determine the EC_{50} of all three molecules on
995 rASIC3 (n = 4-12, GMQ EC_{50} = 0.68 mM; GBZ EC_{50} = 67.5 μM; sephin1 EC_{50} =
996 1.22 mM). (F inset) Magnification of the concentration-response curves of all
997 three drugs.
998
999 **Fig. 5. Effect of sephin1 on rASIC3 response to mild acidosis (pH 7) and pH-**
1000 **dependency**. (A) Concentration-response effect of increasing concentrations of
1001 sephin1 (1μM–1mM) applied at pH 7 on rASIC3. (B) Fitting of normalised values
1002 for the transient (peak) and sustained current (pA/pF) obtained in A using a
1003 sigmoidal function. (C and D) Bar plot showing the quantification of the data
1004 points obtained in A for each sephin1 concentration. Normalised values were
1005 expressed as a percentage of the baseline rASIC3 pH 7 activation (n = 8-11,
1006 paired t-test, **p ≤ 0.01, ***p ≤ 0.005, ****p ≤ 0.001, vs baseline pH 7 activation).
1007 (E and F) pH-dependent effect of sephin1 on rASIC3. Example traces of rASIC3
1008 response to a pH range from 7.4 to 5 with and without sephin1 (500 μM) (n = 7-
1009 11) (E and F insets) pH-response curves of rASIC3 activation by different pH
1010 extracellular solutions used with (E inset) and without (F inset) sephin1 (500 μM).
1011 (H) Bar plot showing the quantification of the normalised sustained current
1012 (pA/pF) elicited by sephin1 at different pH solutions.
1013
1014 **Fig. 6. Proposed binding site and binding modes of Sephin1 on rASIC3**
1015 **models representing possible closed, open and desensitized**
1016 **conformations.** (A, C and E) Representative top-ranked poses of GMQ (red)
1017 and sephin1 (purple) obtained through AutoDock 4.2.6-based blind docking
1018 against rASIC3-closed, rASIC3-open and rASIC3-desensitized models are
1019 shown. For clarity, only two subunits of the channel are shown in cartoon
1020 representations (subunit A in golden colour and subunit C in pale blue colour). A
1021 close-up view of the site and the docked poses is shown to the left. (B, D and F).
1022 PoseView™-derived ligand interaction diagrams for the docked poses of sephin1

1023 and GMQ for each model are shown. A and C indicate the two subunits of rASIC3-
1024 closed model.
1025
1026 **Fig. 7. Docking of GMQ, GBZ and sephin1 to the rASIC3-closed, rASIC3-**
1027 **open and rASIC3-desensitized homology models.** (A, C and E) Typical top 5
1028 docked poses of selected drugs obtained through AutoDock 4.2.6-based blind
1029 docking against rASIC3 models that are likely to represent various states of the
1030 channel: rASIC3-closed (A), rASIC3-open (B) and rASIC3-desensitized (C). For
1031 clarity, only two subunits of the channel are shown in cartoon representations
1032 (subunit A in golden colour and subunit C in pale blue colour). For all panels, the
1033 top-ranked pose of GMQ, GBZ and Sephin1 are shown as red, green and purple,
1034 respectively. The second, third, fourth and fifth poses for each drug are shown in
1035 yellow, cyan, blue and orange red colour. Images were prepared using UCSF
1036 Chimera version 1.14.
1037
1038 **Table 1. Effect of the selected compounds applied at pH 7 on rASIC3**
1039 **activation**. Comparison of the mean ± SEM of the amplitude of the transient
1040 (I_{peak}) and sustained current (I_{5s}), together with the ratio I_{5s}/I_{peak} between baseline
1041 rASIC3 pH 7 response and after application of each compound at pH 7 (Paired t-
1042 test, *$p \leq 0.05$, **$p \leq 0.01$, ***$p \leq 0.005$, ****$p \leq 0.0001$).
1043
1044 **Table 2. Effect of the preapplication of the selected compounds on rASIC3**
1045 **current kinetics**. Comparison of the mean ± SEM of the amplitude of the
1046 transient (I_{peak}) and sustained (I_{5s}) current, together with the ratio I_{5s}/I_{peak} and the
1047 inactivation time constant (Tau) between baseline rASIC3 pH 6 responses and
1048 after compound application (Paired t-test, *$p \leq 0.05$, **$p \leq 0.01$, ***$p \leq 0.005$).

Figure 1

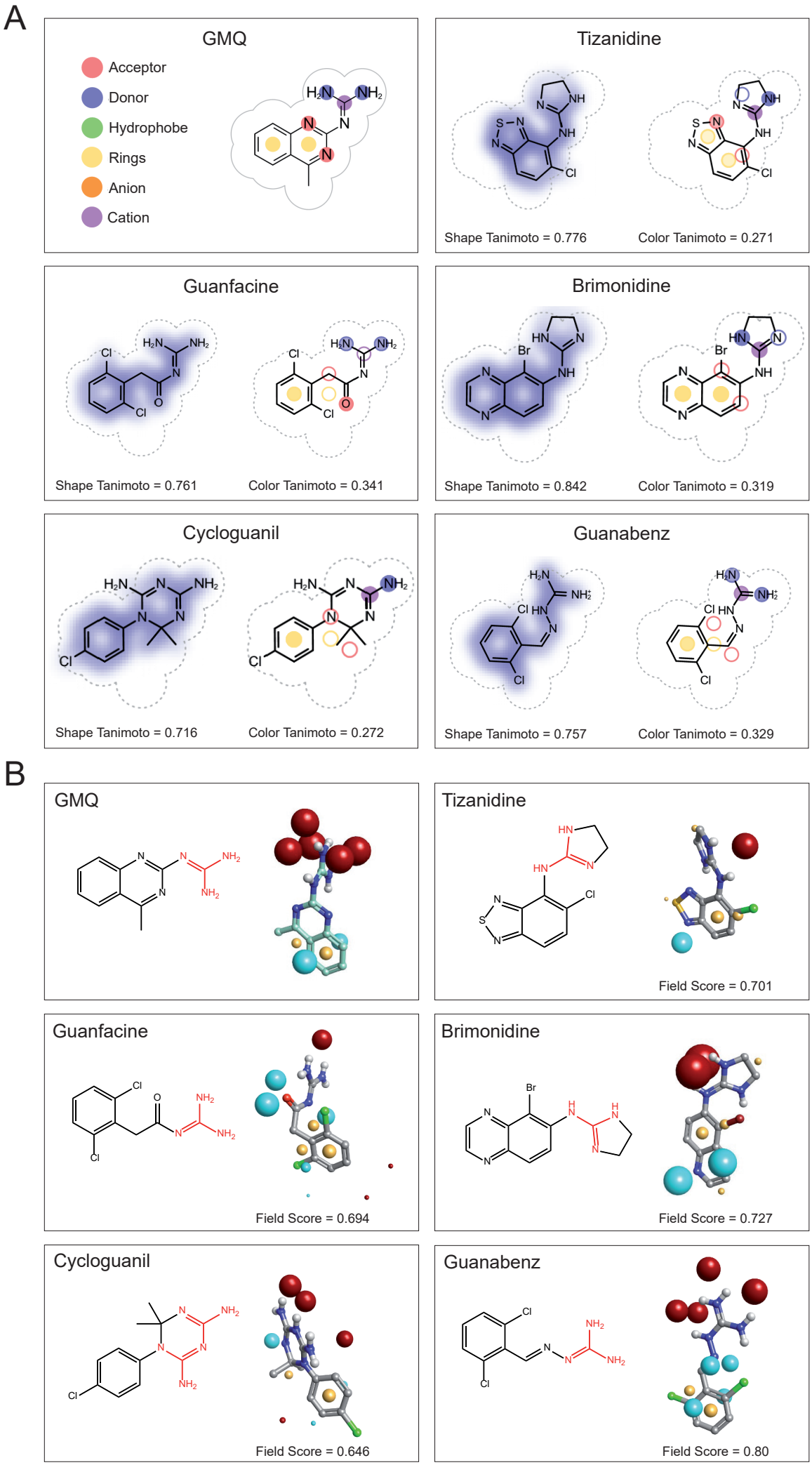
A
GMQ
Acceptor
Donor
Hydrophobe
Rings
Anion
Cation
Tizanidine
Shape Tanimoto = 0.776
Color Tanimoto = 0.271
Guanfacine
Shape Tanimoto = 0.761
Color Tanimoto = 0.341
Brimonidine
Shape Tanimoto = 0.842
Color Tanimoto = 0.319
Cycloguanil
Shape Tanimoto = 0.716
Color Tanimoto = 0.272
Guanabenz
Shape Tanimoto = 0.757
Color Tanimoto = 0.329
B
GMQ
Tizanidine
Field Score = 0.701
Guanfacine
Field Score = 0.694
Brimonidine
Field Score = 0.727
Cycloguanil
Field Score = 0.646
Guanabenz
Field Score = 0.80

Figure 2

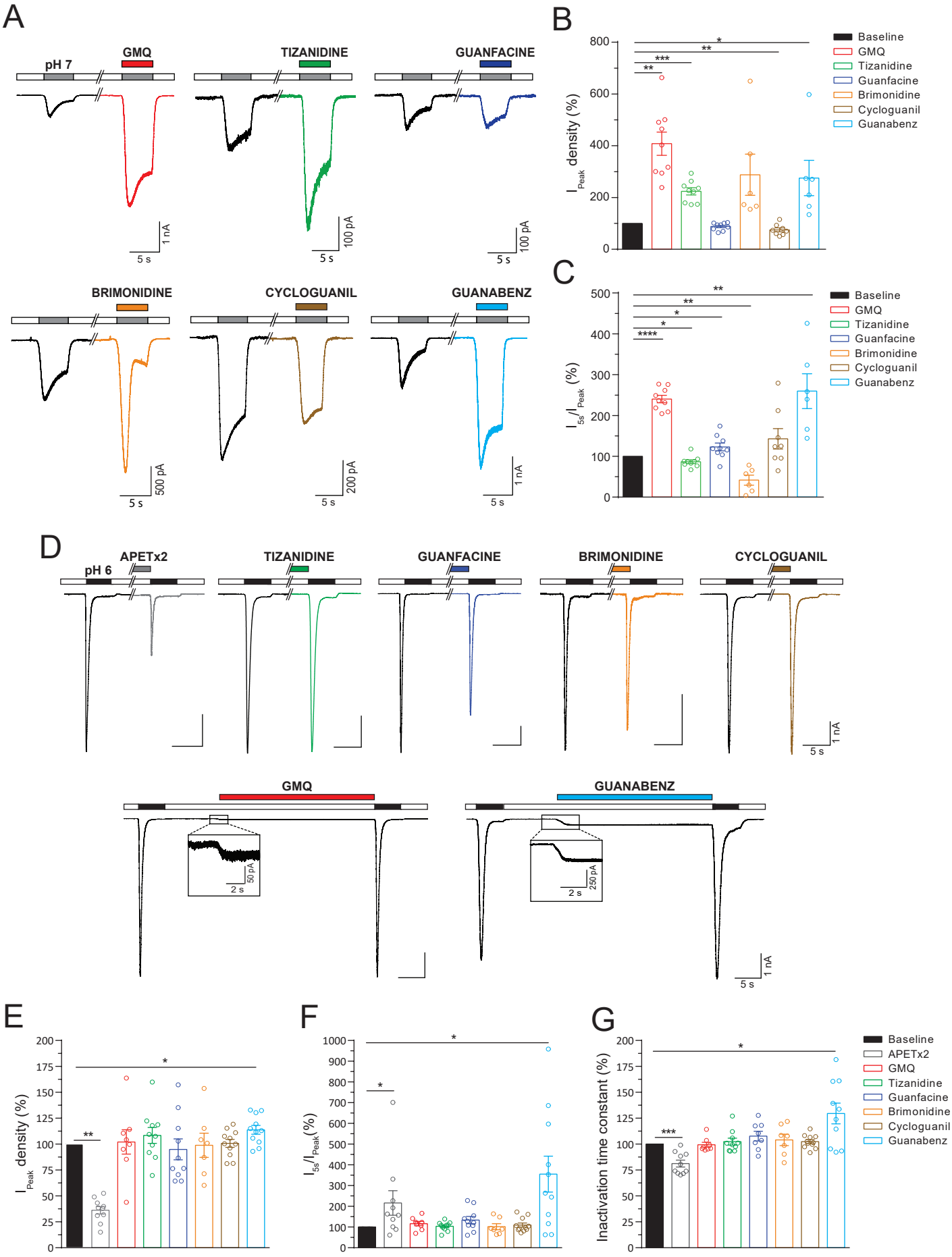
A
pH 7
GMQ
TIZANIDINE
GUANFACINE
BRIMONIDINE
CYCLOGUANIL
GUANABENZ
1 nA
100 pA
500 pA
200 pA
5 s
B
I_{Peak} density (%)
C
I_{5s}/I_{Peak} (%)
Baseline
GMQ
Tizanidine
Guanfacine
Brimonidine
Cycloguanil
Guanabenz
D
pH 6
APETx2
50 pA
250 pA
2 s
E
F
G
Inactivation time constant (%)
APETx2

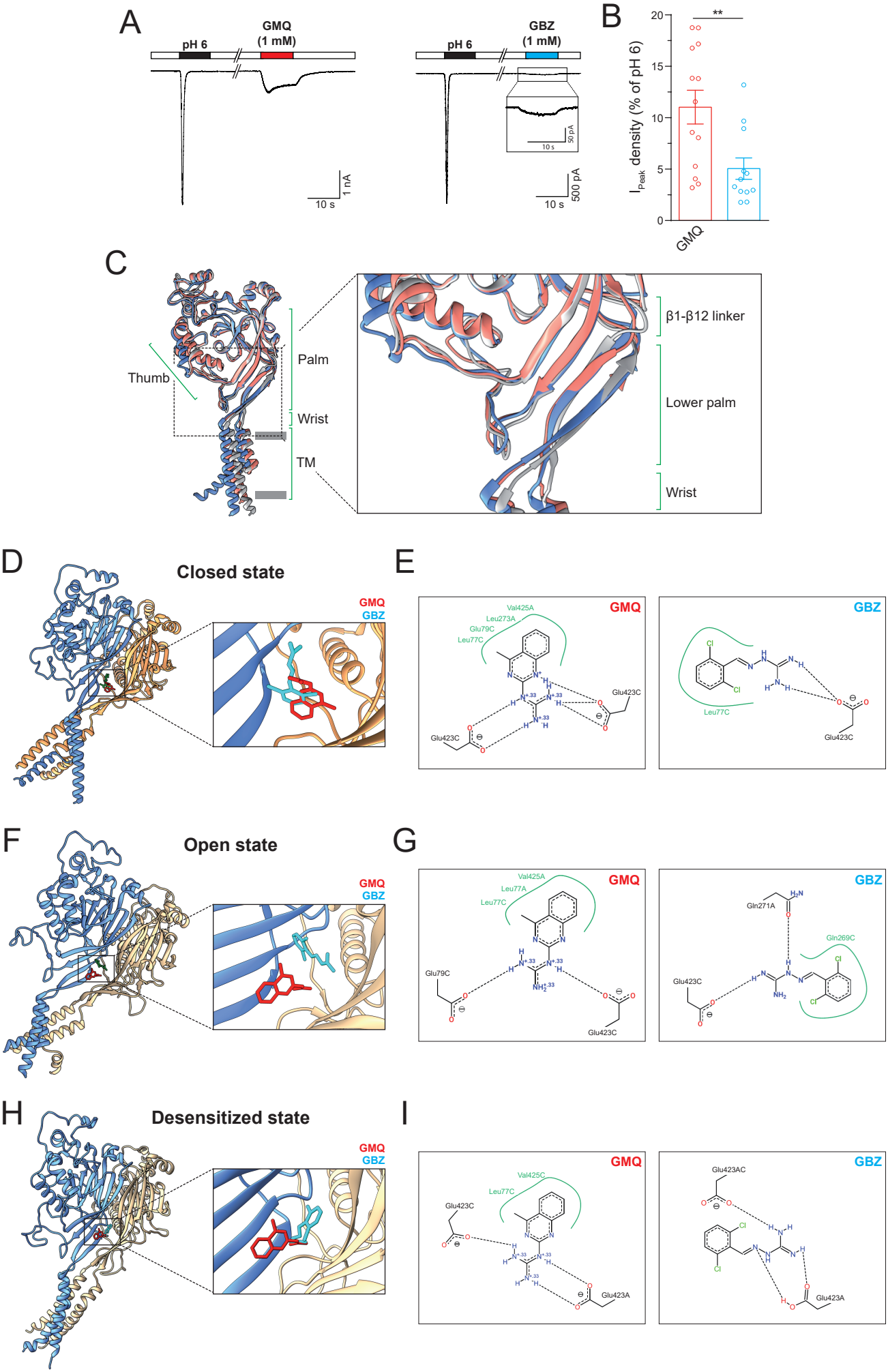
A
pH 6
GMQ
(1 mM)
1 nA
10 s
pH 6
GBZ
(1 mM)
50 pA
10 s
500 pA
10 s
B
**
I_{Peak} density (% of pH 6)
20
15
10
5
0
GMQ
C
Thumb
Palm
Wrist
TM
β1-β12 linker
Lower palm
Wrist
D
Closed state
GMQ
GBZ
E
GMQ
Val425A
Leu273A
Glu79C
Leu77C
Glu423C
Glu423C
GBZ
Cl
Cl
Leu77C
Glu423C
F
Open state
GMQ
GBZ
G
GMQ
Val425A
Leu77A
Leu77C
Glu79C
Glu423C
GBZ
Gln271A
Gln269C
Glu423C
H
Desensitized state
GMQ
GBZ
I
GMQ
Val425C
Leu77C
Glu423C
Glu423A
GBZ
Glu423AC
Cl
Cl
Glu423A

Figure 4

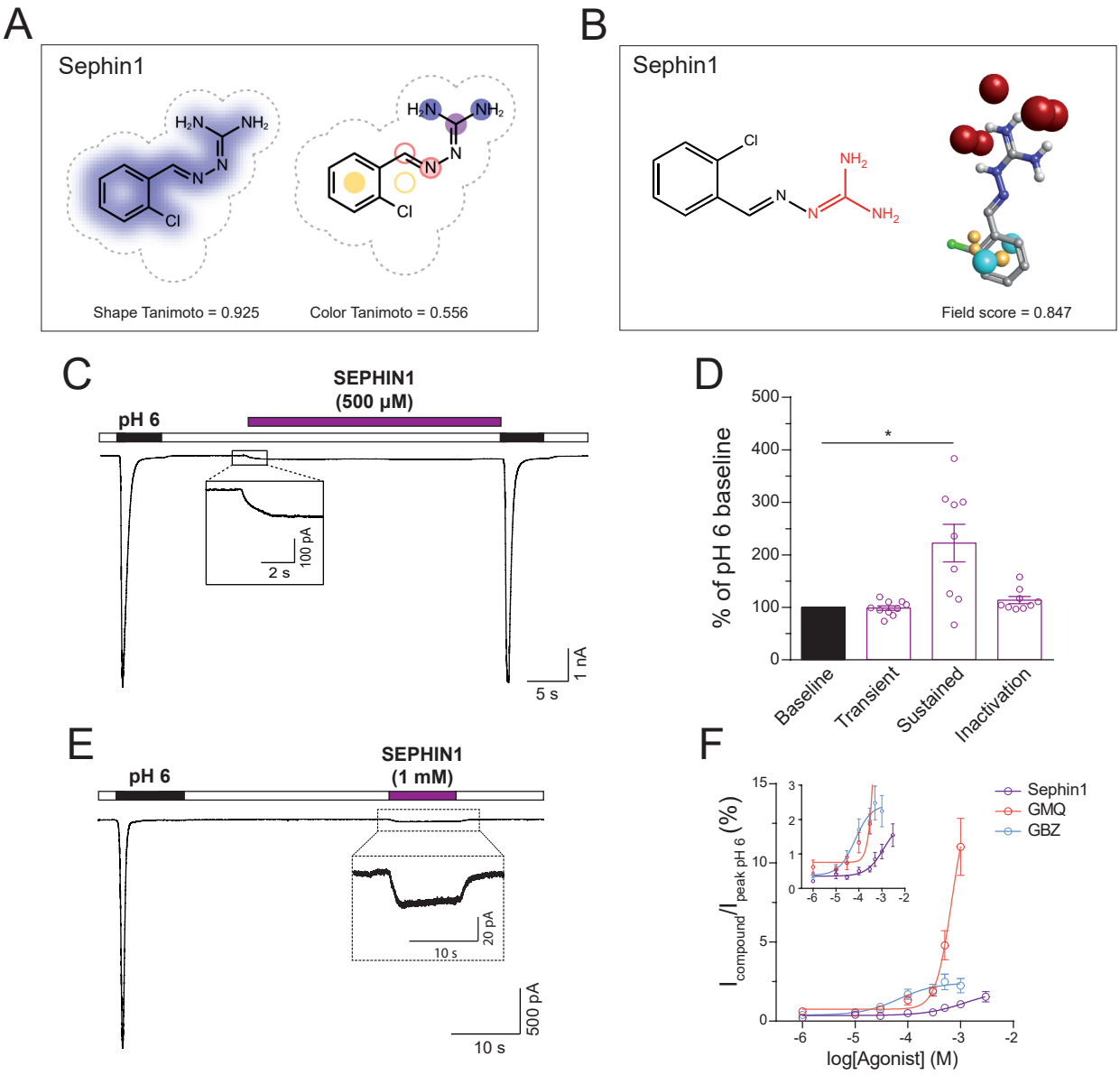
A
Sephin1
Shape Tanimoto = 0.925
Color Tanimoto = 0.556
B
Sephin1
Field score = 0.847
C
SEPHIN1
(500 μM)
pH 6
100 pA
2 s
1 nA
5 s
D
% of pH 6 baseline
Baseline
Transient
Sustained
Inactivation
E
SEPHIN1
(1 mM)
pH 6
20 pA
10 s
500 pA
10 s
F
Sephin1
GMQ
GBZ
log[Agonist] (M)

Figure 5

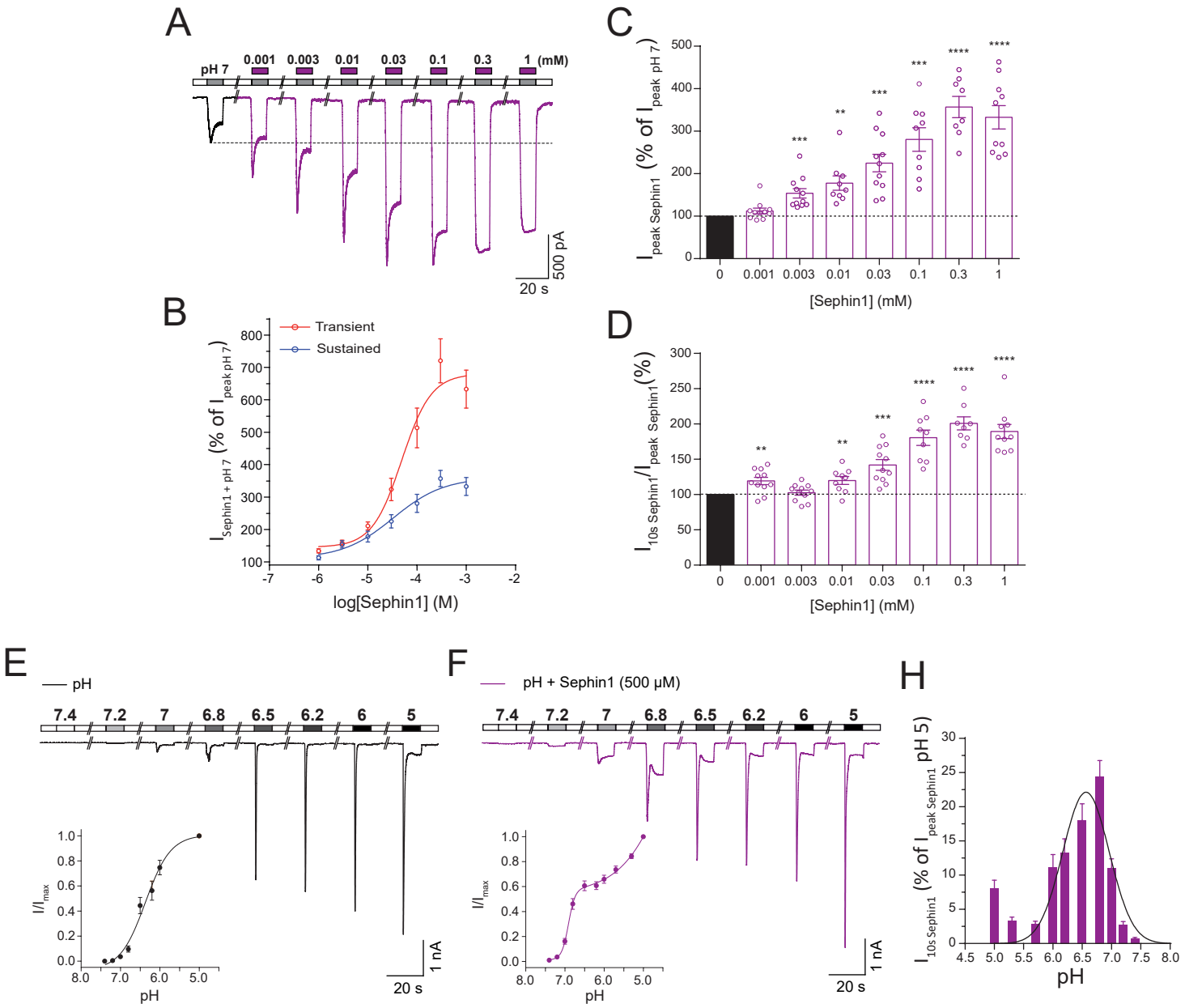
A
pH 7
0.001
0.003
0.01
0.03
0.1
0.3
1 (mM)
500 pA
20 s
B
Transient
Sustained
$I_{Sephin1 + pH 7}$ (% of $I_{peak\ pH 7}$)
log[Sephin1] (M)
C
$I_{peak\ Sephin1}$ (% of $I_{peak\ pH 7}$)
[Sephin1] (mM)
D
$I_{10s\ Sephin1}/I_{peak\ Sephin1}$ (%)
[Sephin1] (mM)
E
pH
7.4
7.2
7
6.8
6.5
6.2
6
5
I/I_{max}
pH
1 nA
20 s
F
pH + Sephin1 (500 µM)
7.4
7.2
7
6.8
6.5
6.2
6
5
I/I_{max}
pH
1 nA
20 s
H
$I_{10s\ Sephin1}$ (% of $I_{peak\ Sephin1}$ pH 5)
pH

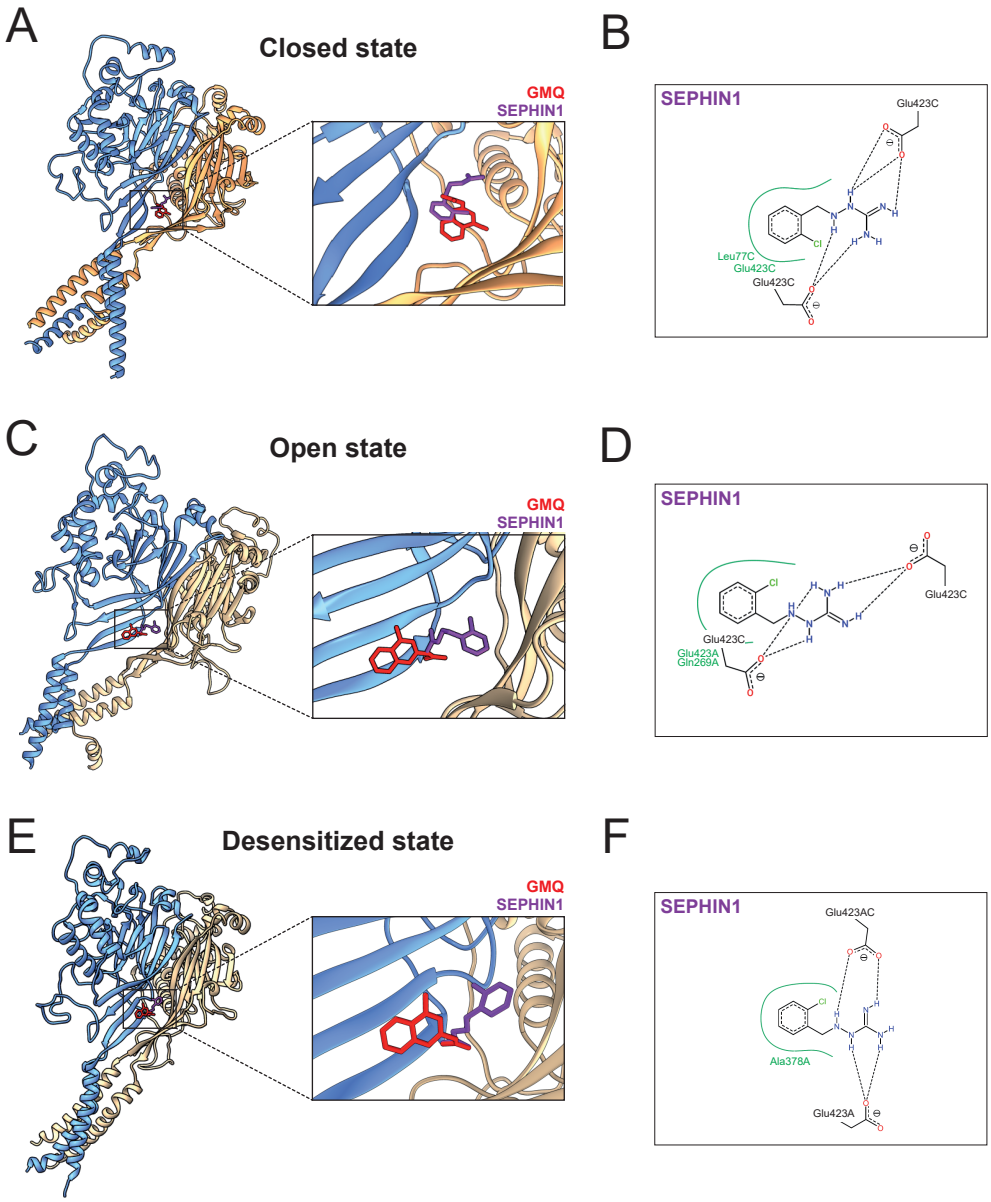
A
Closed state
GMQ
SEPHIN1
B
SEPHIN1
Glu423C
Leu77C
Glu423C
Glu423C
C
Open state
GMQ
SEPHIN1
D
SEPHIN1
Glu423C
Glu423C
Glu423A
Gln269A
E
Desensitized state
GMQ
SEPHIN1
F
SEPHIN1
Glu423AC
Ala378A
Glu423A

Figure 7

A

Closed state

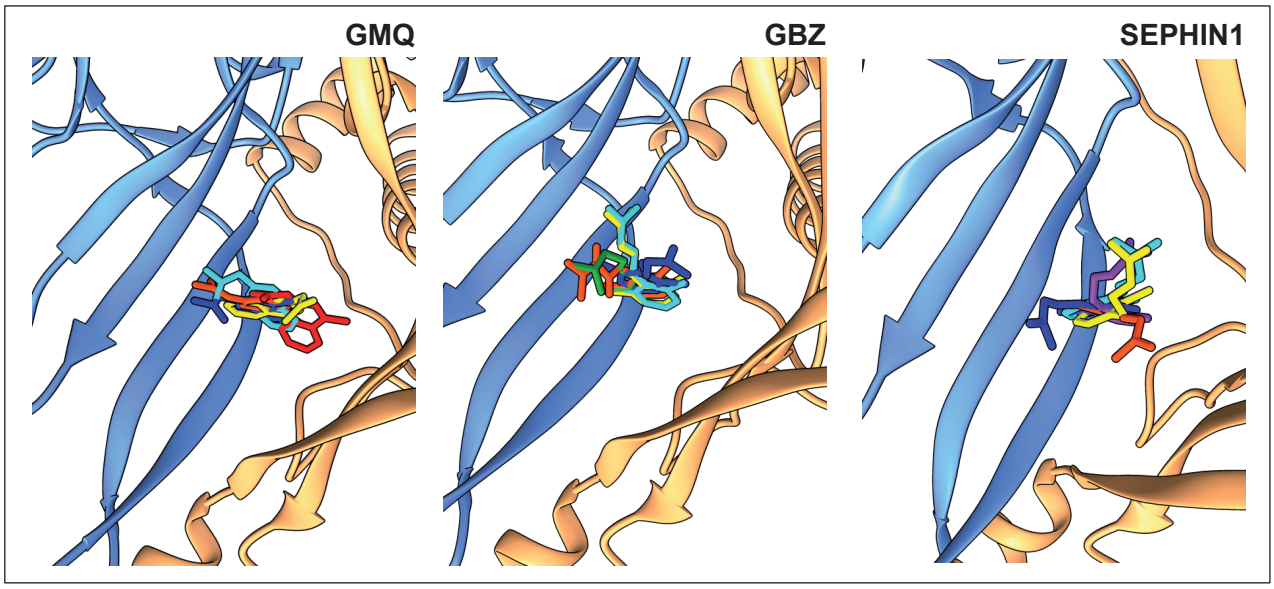

B

Open state

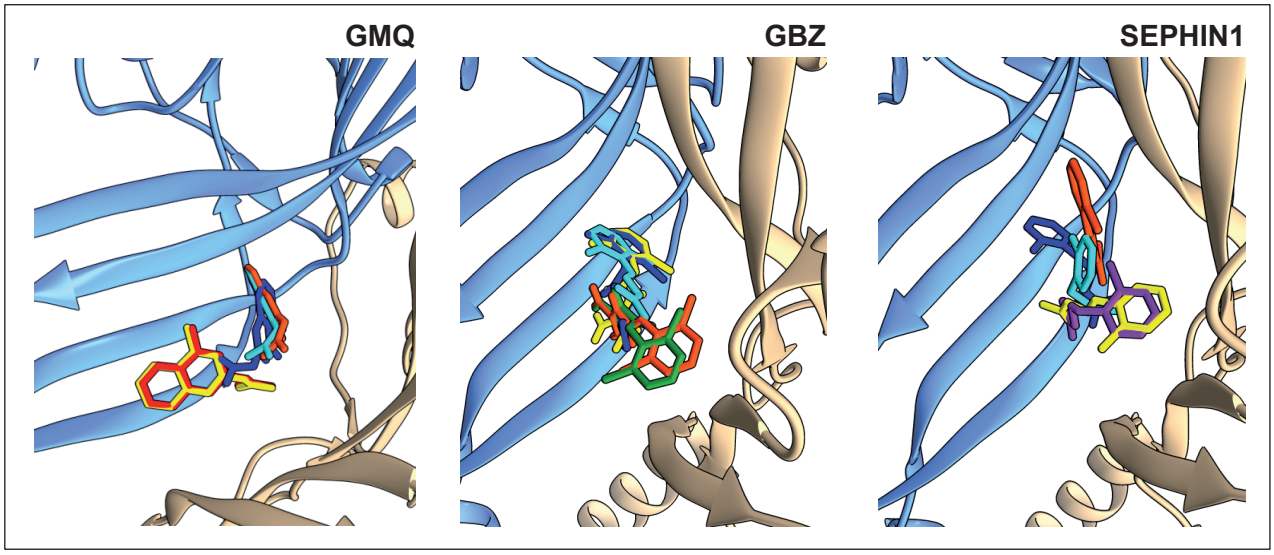

C

Desensitized state

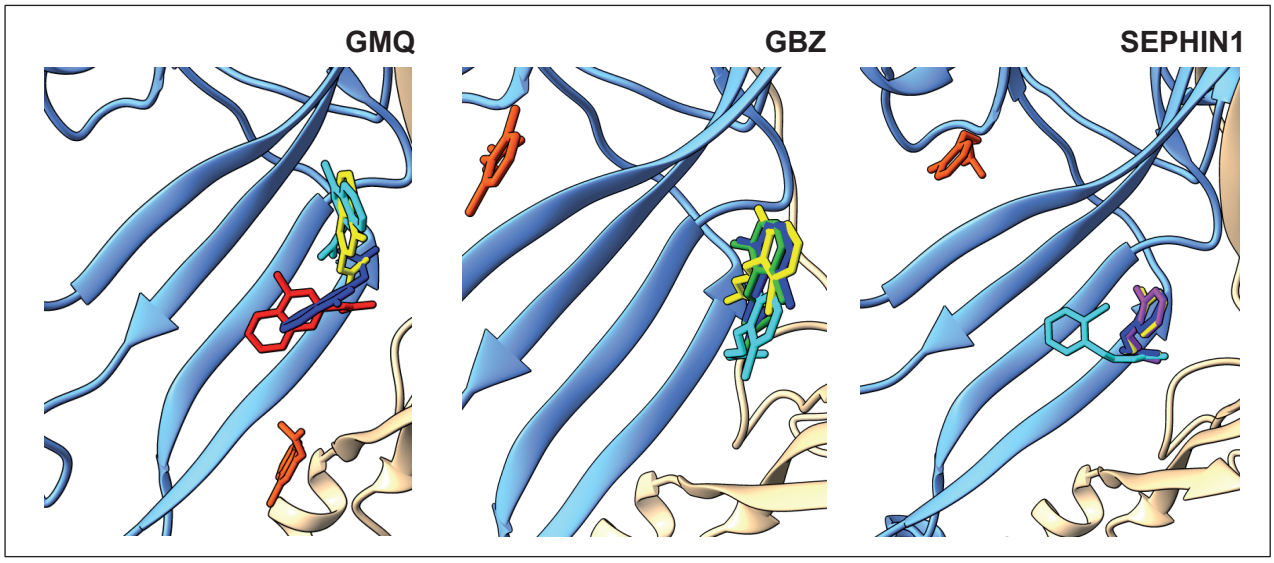

Table 1

	I_{Peak} (pA/pF)		I_{5s} (pA/pF)		I_{5s}/I_{Peak} (%)	
	Baseline	**Compound effect**	**Baseline**	**Compound effect**	**Baseline**	**Compound effect**
GMQ (n = 9)	50.06 ± 5.96	203.43 ± 34.87**	13.36 ± 1.58	132.51 ± 25.41**	26.81 ± 1.2	63.78 ± 1.99****
Tizanidine (n = 9)	32.32 ± 3.68	73.75 ± 10.8***	19.56 ± 3.38	38.87 ± 7.39**	73.66 ± 7.93	63.4 ± 6.72*
Guanfacine (n = 9)	46.41 ± 8.62	40.34 ± 6.69	28.93 ± 6.34	30.65 ± 6.35	60.39 ± 4.89	71.5 ± 4.66*
Brimonidine (n = 6)	83.42 ± 23.27	230.46 ± 75.4	52.25 ± 13.84	38.53 ± 11.8	63.64 ± 4.72	25.33 ± 7.24**
Cycloguanil (n = 8)	83.95 ± 22.82	65.21 ± 22.02**	31.64 ± 7.94	28.42 ± 6.26	43.54 ± 8.19	53.95 ± 7.44
Guanabenz (n = 6)	159.36 ± 36.07	418.64 ± 103.5*	52.31 ±9.6	342.16 ± 82.59*	35.06 ± 4.93	81.3 ± 3.2**

Table 2

	I_{Peak} (pA/pF)		I_{5s} (pA/pF)		I_{5s}/I_{Peak} (%)		Tau (ms)	
	Baseline	**Compound effect**	**Baseline**	**Compound effect**	**Baseline**	**Compound effect**	**Baseline**	**Compound effect**
APETx2 (n = 10)	895.55 ± 160.39	301.01 ± 48.83**	5.76 ± 1.17	3.52 ± 0.77*	0.92 ± 0.34	1.53 ± 0.54*	303.12 ± 14.55	243.82 ± 10.06***
GMQ (n = 8)	747.04 ± 107.29	746.18 ± 118.3	2.74 ± 0.36	2.9 ± 0.29	0.40 ± 0.06	0.47 ± 0.09	307.2 ± 16.01	307.36 ± 23.19
Tizanidine (n = 10)	806.1 ± 44.39	866.66 ± 68.76	8.65 ± 1.19	9.25 ± 1.2	1.09 ± 0.14	1.14 ± 0.2	311.15 ± 15.68	318.14 ± 18.60
Guanfacine (n = 10)	1110.47 ± 90.16	1040.74 ± 119.5	7.68 ± 1.27	8.19 ± 1.06	0.68 ± 0.09	0.85 ± 0.14	318.97 ± 21.26	349.97 ± 25.79
Brimonidine (n = 7)	1044.28 ± 102.4	1023.4 ± 144.2	9.4 ± 2.1	8.38 ± 1.85	1.03 ± 0.3	0.93 ± 0.25	290.49 ± 19.13	304.18 ± 31.09
Cycloguanil (n = 11)	1035.98 ± 94.33	1055.7 ± 122.5	15.32 ± 5.77	15.09 ± 5.3	1.27 ± 0.35	1.22 ± 0.28	319.34 ± 8.47	326.95 ± 10.56
Guanabenz (n = 11)	681.83 ± 78.52	773.52 ± 95.37*	9.85 ± 2.32	28.33 ± 6.81*	1.56 ± 0.5	3.92 ± 0.73*	319.45 ± 13.85	415.38 ± 36.55*
Sephin1 (n = 10)	782.88 ± 98.52	775.13 ± 108.72	4.33 ± 0.65	11.28 ± 2.88*	0.65 ± 0.13	1.92 ± 0.62	301.44 ± 16.56	336.91 ± 34.40